Certain ortho-hydroxylated brominated ethers are promiscuous kinase inhibitors that impair neuronal signaling and neurodevelopmental processes

Received for publication, September 18, 2019, and in revised form, March 23, 2020 Published, Papers in Press, March 30, 2020, DOI 10.1074/jbc.RA119.011138

Robert G. Poston[‡], Lillian Murphy[§], Ayna Rejepova[‡], Mina Ghaninejad-Esfahani[‡], Joshua Segales[‡], Kimberly Mulligan[§], and Ramendra N. Saha[‡1]

From the [‡]Molecular and Cell Biology Department, School of Natural Sciences, University of California, Merced, Merced, California 95343 and the [§]Department of Biological Sciences, Center for Interdisciplinary Molecular Biology: Education, Research and Advancement (CIMERA), California State University, Sacramento, California 95819

Edited by Roger J. Colbran

The developing nervous system is remarkably sensitive to environmental signals, including disruptive toxins, such as polybrominated diphenyl ethers (PBDEs). PBDEs are an environmentally pervasive class of brominated flame retardants whose neurodevelopmental toxicity mechanisms remain largely unclear. Using dissociated cortical neurons from embryonic *Rattus norvegicus*, we found here that chronic exposure to 6-OH–BDE-47, one of the most prevalent hydroxylated PBDE metabolites, suppresses both spontaneous and evoked neuronal electrical activity. On the basis of our previous work on mitogen-activated protein kinase (MAPK)/extracellular signal-related kinase (ERK) (MEK) biology and our observation that 6-OH–BDE-47 is structurally similar to kinase inhibitors, we hypothesized that certain hydroxylated PBDEs mediate neurotoxicity, at least in part, by impairing the MEK–ERK axis of MAPK signal transduction. We tested this hypothesis on three experimental platforms: 1) *in silico*, where modeling ligand–protein docking suggested that 6-OH–BDE-47 is a promiscuous ATP-competitive kinase inhibitor; 2) *in vitro* in dissociated neurons, where 6-OH–BDE-47 and another specific hydroxylated BDE metabolite similarly impaired phosphorylation of MEK/ERK1/2 and activity-induced transcription of a neuronal immediate early gene; and 3) *in vivo* in *Drosophila melanogaster*, where developmental exposures to 6-OH–BDE-47 and a MAPK inhibitor resulted in offspring displaying similarly increased frequency of mushroom-body β–lobe midline crossing, a metric of axonal guidance. Taken together, our results support that certain ortho-hydroxylated PBDE metabolites are promiscuous kinase inhibitors and can cause disruptions of critical neurodevelopmental processes, including neuronal electrical activity, presynaptic functions, MEK–ERK signaling, and axonal guidance.

Humans around the world face exposure to a vast number of anthropogenic environmental contaminants that are largely untested for safety, many in the form of industrial chemicals. Use of one such class of environmentally-widespread flame retardants, polybrominated diphenyl ethers (PBDEs),[2] began in the 1970s in response to regulatory efforts concerning fire-related safety of consumer products. They are now known to be stable in the environment and highly lipophilic, enabling collection in household dust and persistent bioaccumulation. The primary route of human exposure is ingestion and inhalation of such dust-borne PBDEs (1, 2), with dietary intake from seafood and dairy products accounting for much of the remaining exposures (3). Exposure levels are known to be high in the United States in particular, with infants and toddlers carrying the highest body burdens due to elevated intake rates from household exposures (4).

PBDEs have also been identified as one of a number of environmental pollutants that are considered developmental neurotoxins (5). Concerningly, a substantial amount of research has established the relationship of PBDE exposure levels with behavioral deficits in humans, as well as in animal models. Recently, several large-scale and systematic reviews have concluded that PBDE exposures impact externalizing behaviors and IQ in children and that BDE-47, -99, and -209 affect learning in animal studies (6–9). There is also concern for the relationship between environmental toxins like PBDEs and autism spectrum disorders, although the evidence is less conclusive, especially in human studies (6, 10–20). Given the prevalence of these compounds and their association with behavioral deficits, it is imperative to understand the molecular and cellular mechanisms underlying PBDE neurotoxicity.

Exposure to PBDEs has been shown to have numerous effects on neural cells, which are thoroughly reviewed elsewhere (21).

This work was supported by National Institutes of Health NIGMS-RISE Grant R25GM122667 for the *Drosophila* portion of the study and by NIEHS Grant R01ES028738 (to R. N. S.). The authors declare that they have no conflicts of interest with the contents of this article. The content is solely the responsibility of the authors and does not necessarily represent the official views of the National Institutes of Health.

This article contains Figs. S1–S4.

[1] To whom correspondence should be addressed: Rm. 346, S & E Bldg. 1, University of California, Merced, 5200 North Lake Road, Merced, CA 95343. Tel.: 209-228-2425; E-mail: rsaha3@ucmerced.edu.

[2] The abbreviations used are: PBDE, polybrominated diphenyl ether; MEK, MAPK/ERK kinase; ERK, extracellular signal-related kinase; MAPK, mitogen-activated protein kinase; IEG, immediate early gene; MEA, microelectrode array; 6-OH, 6-OH–BDE-47; DIV, days *in vitro*; Bic, bicuculline; ANOVA, analysis of variance; PMA, phorbol 12-myristate 13-acetate; TTX, tetrodotoxin; ICKP, International Centre for Kinase Profiling; CaMKK, Ca^{2+}/calmodulin-dependent protein kinase kinase; BDE, brominated diphenyl ether; PD, PD0325901; aNSC, adult neural stem cell; PKC, protein kinase C; HBSS, Hanks' balanced salt solution; PVDF, polyvinylidene difluoride; 4AP, 4-aminopyridine; IP, immunoprecipitation; NDD, neurodevelopmental disorder.

Several of the major known mechanisms of PBDE toxicity include the following: 1) interference with endocrine signaling, likely caused by structural similarities to thyroid hormones and other hormone receptors' ligands (22–25); 2) disruptions of calcium homeostasis/signaling as shown in one of the earliest mechanistic studies of PBDEs (26) and more recently demonstrated in several cell types, including human neuronal precursors (27, 28); 3) toxicity produced by mitochondrial disruptions, including uncoupling of oxidative phosphorylation (29) and subsequent elevated production of reactive oxygen species that can lead to DNA damage and apoptosis; and 4) dysregulation of epigenetic mechanisms, including DNA methylation, chromatin dynamics, and noncoding RNAs—an emerging point of investigation that we have recently reviewed (30). It is possible that one or more of these molecular mechanisms contribute to exposure-related behavioral abnormalities; however, the extent of their involvement, if any, remains unclear.

The complex nature of the effects of these toxins is likely due in part to their diversity; there are 209 PBDE congeners, many found in commercial flame-retardant mixtures, and these compounds can be further endogenously metabolized in our cells. Such metabolism, mediated in humans by cytochrome P450 enzymes (31–33) and inherent in some other natural contexts (34–37), leads to the production of hydroxylated and methoxylated forms of PBDEs. In addition to parent congeners, toxicity may also arise from these metabolic products of PBDEs, some of which (*e.g.* 6-OH–BDE-47) have been found to be more toxic than the parent compound (25, 27). Given the numerous PBDEs to which humans are exposed, including these metabolized forms, understanding how the effects of exposures to various PBDEs impact neurodevelopmental processes has been a difficult process, and it is likely that unreported mechanisms are involved.

Previously, we have utilized the ability of neurons to induce gene transcription in response to elevated network activity as a tool for assessing developmental PBDE toxicity (38). Specifically, we assayed levels of the neuron-specific activity-induced immediate early gene (IEG) *Arc* after exposing embryonic cortical neurons across various stages of differentiation and maturation. Our rationale for employing this end point was that *Arc* induction relies on multiple levels of regulation, from electrical activity and synaptic function to intracellular signaling (particularly Ca^{2+}-dependent mechanisms) and to nuclear regulation of gene expression, all of which are critical processes intertwined in regulating neurodevelopment (39). These processes are largely hardwired by genetic programs but are also modulated by environmental cues. Exposure to toxins like PBDEs represents an environmental challenge that may dysregulate these processes at multiple levels, the cumulative effects of which could be detected as altered transcriptional responses. Results from our previous study showed that chronic exposures to a hydroxylated metabolite of BDE-47, 6-OH–BDE-47 (6-OH), dysregulate basal and activity-dependent neuronal transcription. Among those findings were data that strongly indicated that the attenuated transcriptional response following 6-OH exposure is due to synaptic dysfunction and that 6-OH is potentially capable of inhibiting intracellular signaling. Either could explain the attenuated transcription of *Arc*, as its activity-induced transcription relies on synaptic activity as well as signaling via the MAPK cascade, one of the major signaling pathways that is important for neuronal plasticity (40) and is necessary for *Arc* induction (41).

In this study, we propose and test a novel mechanism of PBDE metabolite toxicity via impairment of MEK–ERK signaling. The notion that a PBDE metabolite could have the capacity to impair MAPK signaling was of particular interest to us for several reasons. The MAPK pathway is a deeply evolutionarily–conserved intracellular signaling mechanism that supports diverse processes in both prokaryotes and eukaryotes (42–44). In prokaryotes, PBDE-mediated inhibition of MAPK-homologous kinases could explain the natural biogenesis of these compounds as a defense mechanism, known to have antimicrobial activity and to be produced by bacteria in several marine contexts, including sponge-cyanobacterial symbiotic relationships (34–37, 45–48). In eukaryotes, the most well-known role of MAPK is regulation of cell growth, division, and differentiation in many cell types, including stem cells in the developing nervous system (49–51). It is also known to regulate axonal guidance and growth that have been demonstrated in multiple species (52–55). Additionally, there are numerous neurodevelopmental disorders (NDDs) that are genetic syndromes involving the dysregulation of Ras and the MAPK pathway, thus known as "RASopathies" (56, 57). In mature neurons—postmitotic nondividing cells—the pathway regulates synaptogenesis (58, 59), synaptic plasticity (60), activity-induced gene expression (41, 61), and generally communicates information to a large number of cellular substrates. These roles in neural cells make MAPK signaling a concerning target for environmental disruption. However, the MAPK pathway remains largely unexplored as a target for pollutants.

With these factors in mind, we sought to expand and clarify our previous findings with the studies reported here. Here, we show that chronic 6-OH exposure suppresses neuronal electrical activity, that 6-OH is a promiscuous kinase inhibitor, and that acute exposures can inhibit MEK–ERK signaling. We also report that *in vivo* exposures to 6-OH and a MEK inhibitor, PD0325901, similarly alter axonal guidance in the mushroom bodies of *Drosophila melanogaster*. These new findings corroborate our earlier work, provide evidence for the novel concept that certain hydroxylated PBDEs are promiscuous kinase inhibitors potentially capable of disrupting cellular processes via a range of intracellular signaling mechanisms, and further demonstrate the ability of PBDE metabolites to disrupt neurodevelopmentally-relevant neuronal processes.

Results

Chronic 6-OH–BDE-47 exposure suppresses electrical activity in cortical neurons

We have previously shown that chronic exposure to nanomolar concentrations of 6-OH–BDE-47 (6-OH) impairs the ability of primary cortical neurons to induce transcription of the IEG *Arc* (38). Findings from that work indicated that the effects of the exposure were manifested at the level of synaptic functionality. To test this hypothesis directly, we utilized the same cell culture system but grew cells on microelectrode

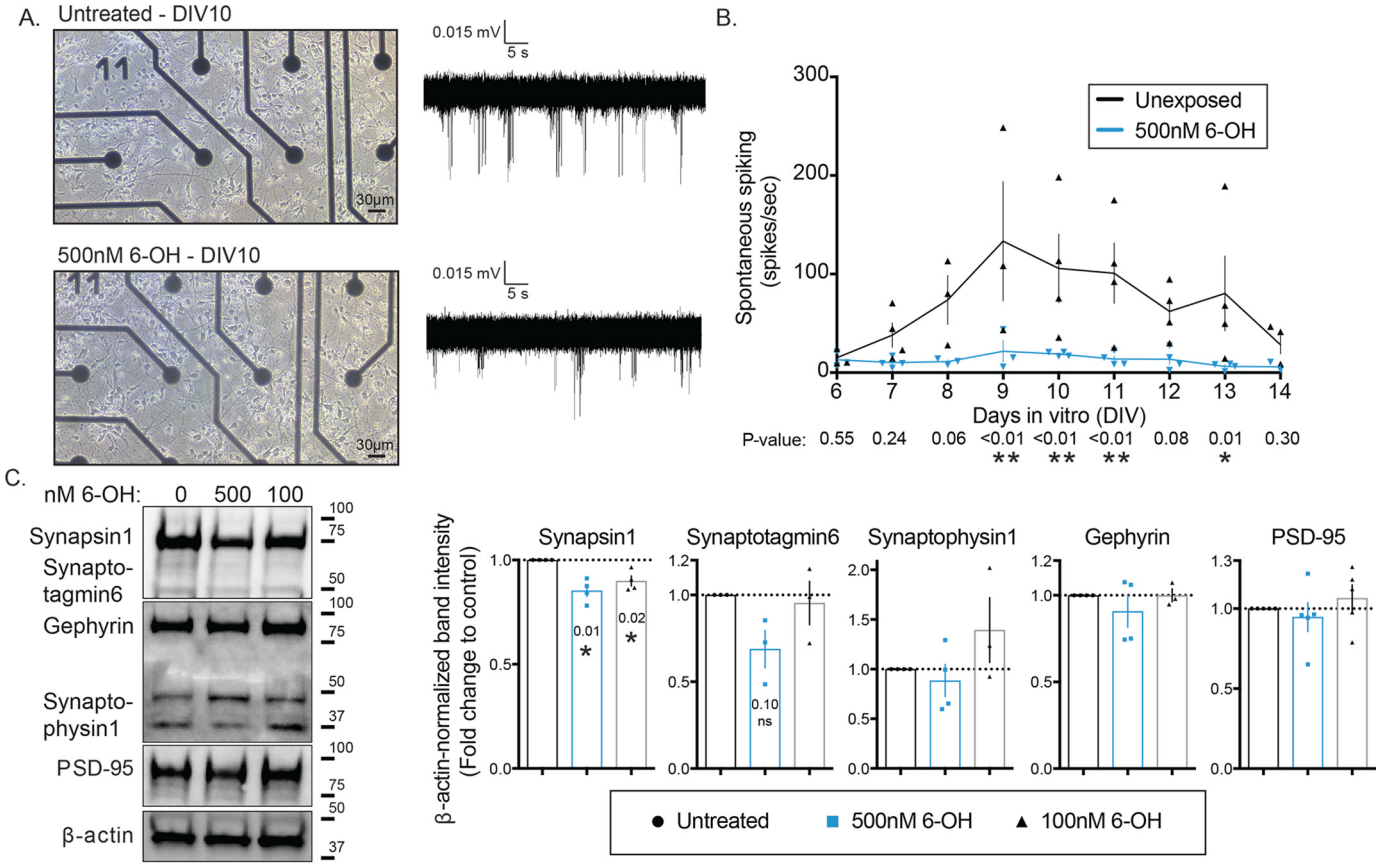

Figure 1. Chronic 6-OH–BDE-47 exposure suppresses spontaneous neuronal activity and alters pre-synapses. Primary rat cortical neurons were grown on MEAs in order to assess the effects of 6-OH exposure on electrical activity. *A,* example images of neurons at DIV10 with or without exposure to 500 nM 6-OH (*left*), and example traces of recorded spontaneous activity (*right*). *B,* detectable activity was measured daily with 3-min recordings and quantified through the first 2 weeks of growth *in vitro*, $n = 3–4$. *p* values were generated with two-way ANOVA with post hoc FDR method. Time $F(8,49) = 2.09$, $p = 0.054$, treatment $F(1,49) = 36.04$, $p < 0.0001$, interaction $F(8,49) = 1.503$, $p = 0.1808$. *C,* synaptosomes were isolated from DIV10 cultures. Pre- and post-synaptic markers were assessed by Western blotting (*left*) and densitometric quantification of blots (*right*) (note: the band between the Gephyrin and Synaptophysin1 is an additional band from the Gephyrin antibody), $n = 3–5$. *p* values were generated with one-sample *t* tests using a hypothetical mean of 1.

arrays (MEAs). Cells were exposed to 500 nM 6-OH from the day of plating, and spontaneous electrical activity of the networks was recorded daily (Fig. 1*A*). There were no obvious morphological differences in cell growth. We also previously demonstrated that this exposure level does not significantly impact cell viability (38). Spontaneous activity was detected usually starting at 6 days *in vitro* (DIV), which is consistent with previous reports for cultured cortical neurons (62), and continued to the end of the experiment at DIV14. Networks exposed to 6-OH displayed significant suppression of spontaneous spiking across the recording period, which was quantified and is summarized in Fig. 1*B*. To further clarify the synaptic nature of the exposure effects, we isolated synaptosomes from 6-OH–treated cultures (DIV0–10) and evaluated the levels of both pre- and post-synaptic protein markers by Western blotting. We found a significant decrease in the amount of detectable Synapsin1, but not several other pre-synaptic proteins or the post-synaptic proteins PSD-95 and gephyrin (Fig. 1*C*). This suggests that the observed activity deficits induced by chronic 6-OH exposure may be specifically mediated by pre-synaptic dysfunction involving synapsin, although effects unrelated to the markers assayed here cannot be ruled out. Together, these data support the hypothesis generated from our earlier work that chronic exposure to the BDE-47–hydroxylated metabolite, 6-OH, impairs synaptic function.

Next, we observed the effects of 6-OH on induced neuronal activity. This was done to partly explain one of our previous observations where activity-induced expression of the IEG *Arc* was significantly reduced in networks chronically exposed to 6-OH (38). To test whether chronic 6-OH exposure impaired firing patterns during induced activity, which could explain impaired *Arc* transcription, we evoked activity in unexposed and 6-OH–exposed networks using two different bicuculline (Bic) stimulation paradigms (Fig. 2*A*). The first was continuous treatment with Bic, similar to the approach we previously used to induce *Arc* transcription (38). The other was a Bic stimulus followed by washout, a treatment paradigm known to produce long-lasting recurrent synchronous bursting that has been previously published as a model of *in vitro* plasticity (63). Both types of Bic treatments produced characteristic burst firing patterns (Fig. 2*B*) that were diminished in 6-OH–treated cells (Fig. 2, *C–F*). The observed reduction in activity after 15 min of continuous Bic treatment (Fig. 2, *C* and *D*) directly explains our earlier finding that chronic 6-OH exposure impairs activity-induced *Arc* transcription due to reduced firing of exposed neurons. The strong effect

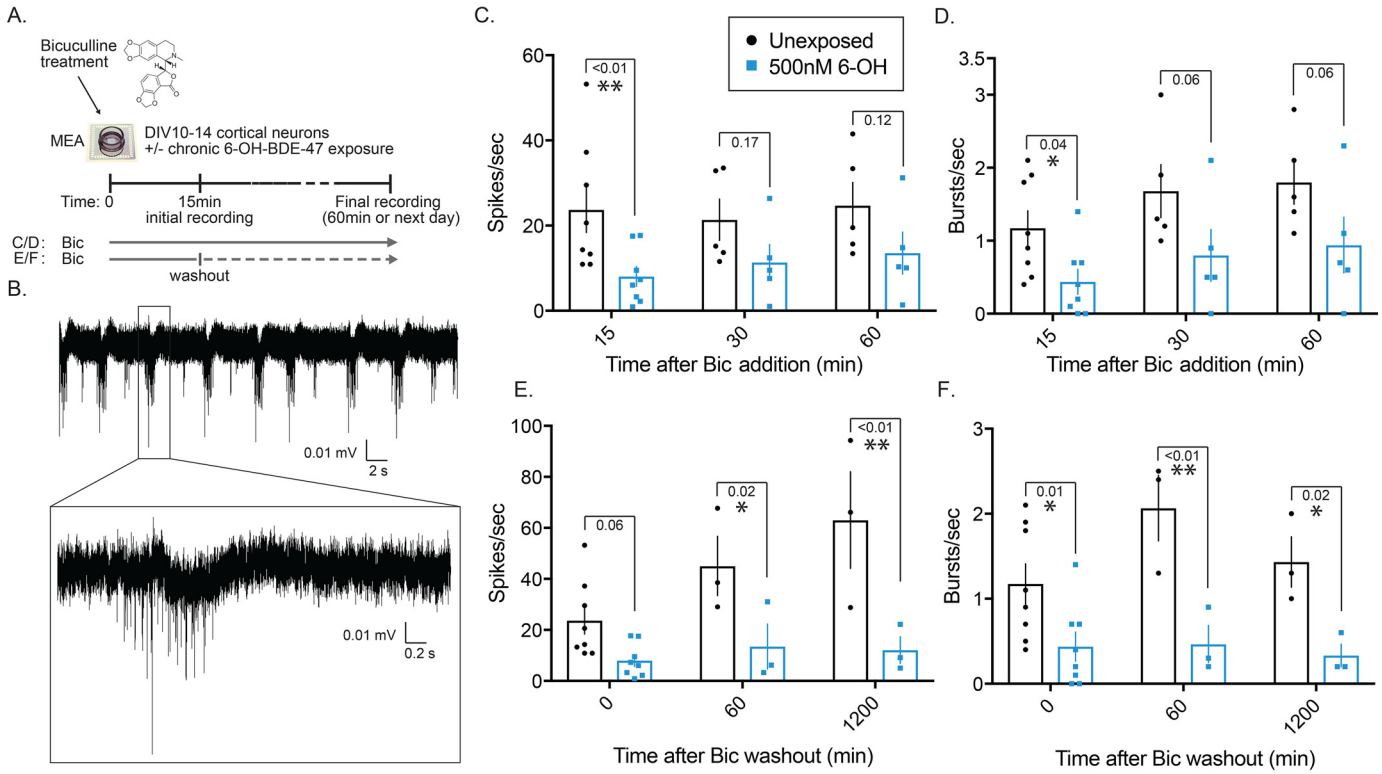

Figure 2. Chronic 6-OH–BDE-47 exposure impairs evoked synaptic activity. Multiple stimulus paradigms were used to assess the effects of chronic 6-OH exposure on evoked electrical activity. *A,* graphical depiction of bicuculline (*Bic*) stimulus paradigms. *B,* example of characteristic burst activity generated with Bic stimulus. *C* and *D*, quantification of spikes and bursts detected under continual Bic treatment of neurons chronically exposed to 500 nM 6-OH (from time of plating to day of experiment), $n = 5–8$. p values were generated with two-way ANOVA with post hoc LSD. Spike data: time $F(2,30) = 0.269$, $p = 0.76$; treatment $F(1,30) = 10.15$, $p = 0.0034$; interaction $F(2,30) = 0.235$, $p = 0.7920$. Burst data: time $F(2,30) = 2.356$, $p = 0.11$; treatment $F(1,30) = 12$, $p = 0.0016$; interaction $F(2,30) = 0.04056$, $p = 0.9603$. *E* and *F*, same experimental design and presentation as in *B*, but after brief Bic stimulation and washout instead of continual treatment, $n = 3–8$. Spike data: time $F(2,22) = 4.62$, $p = 0.021$; treatment $F(1,22) = 24.31$, $p < 0.0001$; interaction $F(2,22) = 2.8$, $p = 0.0825$. Burst data: time $F(2,22) = 1.57$, $p = 0.23$; treatment $F(1,22) = 25.03$, $p < 0.0001$; interaction $F(2,22) = 1.393$, $p = 0.2695$.

seen under the Bic washout paradigm (Fig. 2, *E* and *F*) further demonstrates the compromised synaptic functionality of 6-OH–treated cells and suggests that 6-OH may specifically impair the molecular mechanisms regulating induction and maintenance of Bic-induced bursting.

6-OH–BDE-47 is a promiscuous kinase inhibitor

The report that previously published the Bic washout paradigm as a model of *in vitro* plasticity also demonstrated that the effect was regulated by MAPK signaling, and could be blocked with a pharmacological MEK inhibitor (63). We additionally found that chronically treating neurons with low concentrations of a similar MEK inhibitor, PD0325901 (PD), impairs spontaneous spiking as well (Fig. S1). Combined with our previous observation that 6-OH is capable of attenuating MAPK-driven gene transcription (38) and the observation that 6-OH shares key structural features with the same class of MEK inhibitors shown to regulate *in vitro* Bic-induced recurrent bursting (Fig. S2*A*), we hypothesized that 6-OH may be capable of directly inhibiting MEK1. To test this hypothesis and to gain insight into the plausibility of 6-OH acting as a small molecule kinase inhibitor, we conducted ligand–protein docking simulations using published crystal structures of MEK1 and 6-OH as well as a commercial inhibitor, PD (a type-III non-ATP competitive inhibitor), which are well-studied (64, 65). Utilizing AutoDock Vina (66), which evaluated energetically-optimized binding poses for each ligand, we found that both 6-OH and PD were placed around the well-characterized allosteric binding pocket for this type of inhibitor, without providing prior information on the binding surface. Almost all of the generated top poses for both 6-OH and PD clustered around this surface when the simulation was initialized near the catalytic kinase domain (Fig. S2*B*). The poses for 6-OH and PD that are closest to the published binding modes of MEK1 inhibitors are superimposed in Fig. S2*C*. These results were encouraging and suggested that 6-OH is capable of realistically interacting with the type of binding surface known to be targeted by small molecules specifically designed to inhibit MEK1.

To our surprise, when we attempted to demonstrate direct MEK1–6-OH binding in a cell-free kinase-inhibition assay, there was no decrease in MEK1 activity across a range of 6-OH concentrations (Fig. 3*B*). However, when we screened a range of kinases, representing much of the human kinome, we found that 6-OH directly reduces the activity of a number of other kinases (Fig. 3*A*). In an attempt to identify shared features that enable the observed promiscuous inhibitory potential of 6-OH, further ligand-docking simulations were conducted with crystal structures of the top hits from the screen (Fig. 3*C*). Interestingly, the top 6-OH binding poses clustered largely in the well-known ATP-binding pockets of each of the modeled kinases. This suggests that 6-OH may, in fact, be a promiscuous ATP-

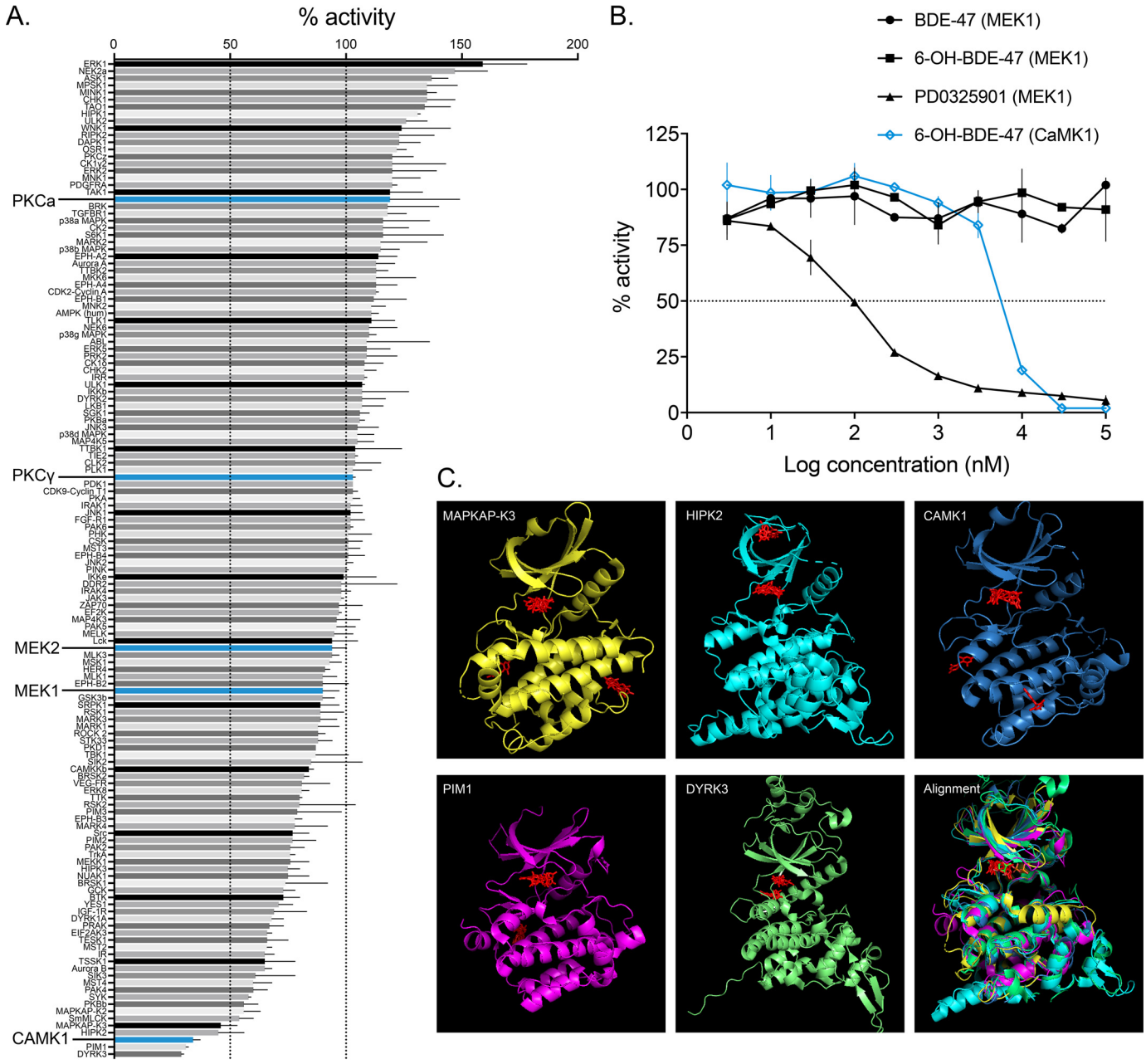

Figure 3. 6-OH–BDE-47 is a promiscuous kinase inhibitor. *A,* 6-OH–BDE-47 was screened against a panel of 140 kinases representing much of the human kinome (screened at 10 μM). *Bars* represent the mean percent activity of each kinase (screened in duplicate), and *error bars* represent standard deviation. The screening method utilizes a published radioactive filter-binding assay using [^{33}P]ATP (110, 111) and was conducted by the International Centre for Kinase Profiling (ICKP) at the University of Dundee. Kinases with enlarged names are of particular interest for their relation to MEK–ERK signaling. *B,* IC_{50} determinations were conducted by the ICKP (using the same methods as cited in *A*) for indicated compounds with either MEK1 or CaMK1. *Error bars* represent standard deviation of each data point, which were conducted in duplicate. No inhibition was observed for BDE-47 or 6-OH with MEK1, whereas the IC_{50} for PD0325901 with MEK1 was detected here as 103 $\pm$ 7 nM, and 6.82 $\pm$ 0.02 μM for 6-OH with CaMK1. It is worth noting that this IC_{50} value for PD is around an order of magnitude higher than previously published, indicating that the estimations presented here may be affected by the sensitivity of this determination method. *C,* ligand-docking simulation results for the top five hits from the kinase screen. Crystal structures were obtained from the Protein Data Bank and are cited under "Materials and methods." Autodock-Vina was used to find energetically-optimal binding poses for 6-OH with each of the kinases, which are displayed in *red* in each panel. The *last panel* displays a structural alignment of the five kinases, with the docking results for CaMK1 superimposed. In each case, top binding poses clustered largely to the well-known ATP-binding pockets of the kinases. 6-OH acting as an ATP-competitive kinase inhibitor may help to explain the complex and diverse effects documented for PBDE exposures.

competitive kinase inhibitor. Two of the top hits from the screen also suggest routes by which 6-OH may indirectly impair MEK–ERK signaling: Dyrk3, which is known to regulate sirtuin activation thereby potentiating ERK activation by insulin signaling (67–69), and intriguingly, CaMK1, which has been shown to regulate depolarization-induced MEK–ERK activity and ERK-regulated long-term potentiation (70–73). Focusing on CaMK1, we found that acute 6-OH exposures completely attenuate phosphorylation levels of a well-known pre-synaptic CaMK1 target, synapsin1–serine 9 (Fig. 3*A*) (74), providing *in vitro* confirmation of CaMK1 inhibition. We also reproduced an effect from a past report on CaMK1–MEK–ERK signaling,

showing that acute exposure to the CaMKK inhibitor STO-609 attenuates depolarization-induced phospho-ERK (pERK) levels (Fig. 3*A*) (70). Given this evidence, we further explored the dynamics of MEK–ERK signaling impairment by hydroxylated PBDE metabolites.

Specific ortho-hydroxylated PBDE metabolite exposures impair MEK–ERK signaling in vitro

In mature neurons, MEK–ERK signaling conveys information to many subcellular locations and substrates, including targets in synapses and the nucleus. To further test the prediction that 6-OH is capable of disrupting MEK–ERK signaling, we acutely exposed primary cortical neurons to BDE-47 and its hydroxylated metabolites and then stimulated them with a treatment of Bic and 4AP. The recurrent bursting driven by this treatment elevates intracellular calcium and induces the MEK–ERK-signaling pathway (driving gene expression and plasticity-related events), which can be detected by measuring the phosphorylation status of both MEK and ERK. In whole-cell extracts, we found that activity-induced elevation of both pMEK and pERK was significantly reduced only in cells treated with 6-OH (Fig. 4*B*), but not the parent compound or its other hydroxylated metabolites. The observed attenuation of pMEK induction is further evidence that 6-OH exerts effects somewhere above MEK in the signaling cascade, which includes CaMK1 as a possibility. As CaMK1 inhibition by 6-OH should only impact depolarization-induced MEK–ERK activation, we assessed the ability of 6-OH– exposed cells to induce pERK when the activation was driven synapse-independently. To do this, we also treated cells with TTX and PMA. This treatment, which is previously described (38) and depicted in Fig. 5*A*, silences propagation of neuronal activity while activating MEK–ERK signaling through protein kinase C (PKC) (which we knew was not inhibited by 6-OH from the kinase screen data). Again, we found that acute exposure only to 6-OH significantly attenuated pERK induction (Fig. 4*C*), indicating that 6-OH likely also impairs MEK–ERK signaling via synapse-independent mechanisms at high concentrations, although to a lesser extent than synapse-driven signaling. Inhibition of a synaptic signaling mechanism, such as CaMK1, could explain the stronger effect seen on synapse-dependent MEK–ERK induction.

Although strong inhibition of MEK–ERK induction was observed with higher 6-OH concentrations that are consistent with the IC_{50} determination for CaMK1 (Fig. 3*B*), the lowest exposure level used (500 nM) was ineffective. The 500 nM dose was of interest to us as we have previously estimated it to be the approximate brain concentration reported from *in vivo* exposure studies of PBDEs in rodents (38) and is on the same order of magnitude as the Environmental Protection Agency–reported average for human exposure (4). As we initially did not see a significant decrease in pMEK/ERK levels with this environmentally-relevant concentration, we exposed cells to 500 nM 6-OH with increasing pre-treatment lengths to test the impact of providing more time for membrane penetrance and intracellular accumulation. This consistently yielded qualitatively mild but statistically insignificant inhibition of pERK in whole-cell extracts (Fig. S3*A*). Considering the subcellular location-specific functions of the MEK–ERK pathway, we next prepared nuclear extracts from neurons treated with 500 nM 6-OH to observe only the amount of pERK entering the nucleus (Fig. S3*B*). Again, we observed mild reduction in pERK levels after acute exposure that was insignificant after quantification. At this point, it appeared that acute 500 nM 6-OH exposures are not sufficient to detectably inhibit high pERK levels induced by the strong Bic + 4AP stimulus. To test the effect of stimulus strength, we activated neurons with 5 μM Bic without 4AP. With this weaker stimulus, we found that acute exposure to 500 nM 6-OH significantly decreased nuclear levels of pERK (Fig. S3*C*).

Next, we measured pre-mRNA levels of the MEK–ERK-dependent and neuron-specific IEG *Arc* after acute PBDE exposure as a second approach to corroborate the above-mentioned pERK induction data. We acutely exposed neurons to BDE-47 and its hydroxylated metabolites as in Fig. 4*B* and found significant attenuation of *Arc* induction only after 6-OH exposure (Fig. 5*B*). We also found that acute exposure to 6-OH significantly attenuated *Arc* induction-driven synapse independently (Fig. 5*C*). Again, the inhibitory effect of 6-OH was stronger on synapse-dependent induction, with significant attenuation of *Arc* induction at all tested doses. With the synapse-independent treatment, the effect was again insignificant with a 500 nM exposure, as with the whole-cell pERK data (Fig. 4), so we again examined whether the strength of the stimulus impacts the extent of inhibition by titrating the concentration of PMA with which the cells were treated. As expected, we found that with a lighter stimulus the extent of 6-OH–induced inhibition was greater, and with *Arc* the pre-mRNA levels were significantly reduced when 500 nM 6-OH– exposed cells were stimulated with 0.01 μM PMA (Fig. 5*D*). Taken together, these data indicate that acute 6-OH exposure impairs MEK–ERK signaling in neurons in dose- and stimulus strength-dependent manners and suggest that signaling in various subcellular locations may be differentially impacted.

To test the generality of our hypothesis regarding how hydroxylated PBDEs like 6-OH can impair MEK–ERK signaling, we acutely exposed cells to several other ortho-hydroxylated PBDE metabolites, whose possession or lack of the substituents hypothesized to mediate kinase inhibition are depicted in Fig. 6*A*. These include BDE-99, the second most environmentally-prevalent PBDE to which humans are exposed (4). It was surprising to find that only one of these ortho-hydroxylates metabolites, 6-OH–BDE-99, reduced pERK induction following Bic treatment (Fig. 6*B*). This metabolite produced nearly an identical effect on *Arc* induction as 6-OH–BDE-47 at various concentrations (Figs. 5*B* and 6*C*). This result suggests that for efficient MEK–ERK impairment, ortho-hydroxylated PBDE metabolites require a para-substituted halogen on the same ring as the hydroxyl group (Fig. 6*A*), potentially explaining why only certain ortho-hydroxylated metabolites impair elevation of pERK levels and subsequent *Arc* transcription.

Axonal guidance is dysregulated in vivo by both 6-OH–BDE-47 and PD0325901

Many developmental and functional processes in neurons are regulated by kinase activity, especially MEK–ERK signaling

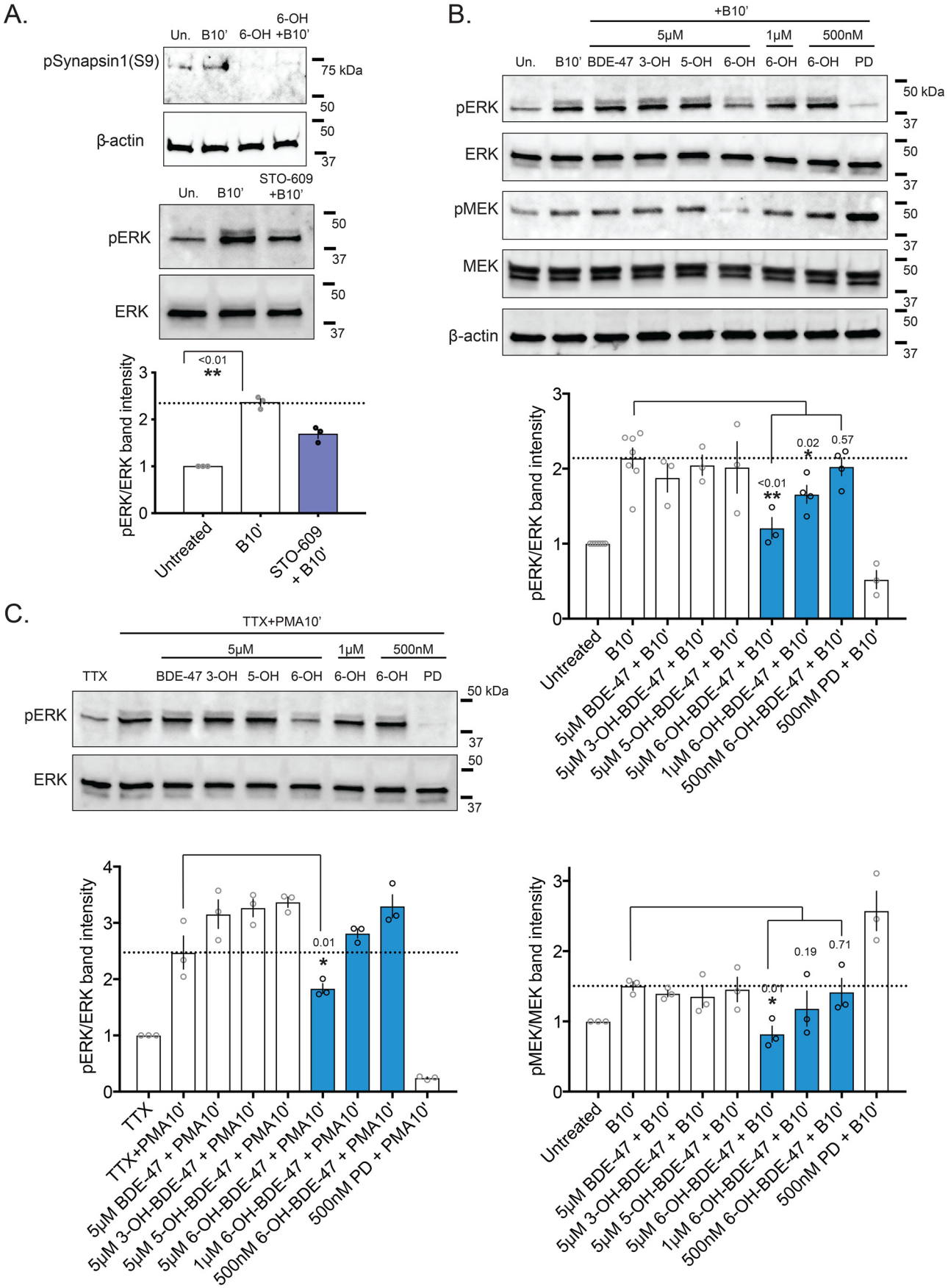
A.
Un.
B10'
6-OH +B10'
pSynapsin1(S9)
75 kDa
50
β-actin
50
37
STO-609 +B10'
pERK
ERK
pERK/ERK band intensity
<0.01
**
Untreated
B10'
STO-609 + B10'
B.
+B10'
5μM
1μM
500nM
BDE-47
3-OH
5-OH
6-OH
PD
pERK
ERK
pMEK
MEK
β-actin
50 kDa
37
pERK/ERK band intensity
0.02
*
0.57
5μM BDE-47 + B10'
5μM 3-OH-BDE-47 + B10'
5μM 5-OH-BDE-47 + B10'
5μM 6-OH-BDE-47 + B10'
1μM 6-OH-BDE-47 + B10'
500nM 6-OH-BDE-47 + B10'
500nM PD + B10'
C.
TTX+PMA10'
TTX
pERK/ERK band intensity
0.01
TTX+PMA10'
5μM BDE-47 + PMA10'
5μM 3-OH-BDE-47 + PMA10'
5μM 5-OH-BDE-47 + PMA10'
5μM 6-OH-BDE-47 + PMA10'
1μM 6-OH-BDE-47 + PMA10'
500nM 6-OH-BDE-47 + PMA10'
500nM PD + PMA10'
pMEK/MEK band intensity
0.19
0.71
0.01

(54, 61, 75). Specifically, it is known to be involved in axonal guidance, along with CaMK1 (73, 76, 77), and that hydroxylated BDEs impact axonal growth *in vitro* (the evidence for which is covered in the discussion). We therefore hypothesized that developmental 6-OH exposures would lead to axonal guidance defects *in vivo*. To test this, we exposed adult flies (*D. melanogaster*) and their offspring to BDE-47, two of its hydroxylated metabolites, and PD. We then assessed axonal guidance in the brains of offspring by observing effects on mushroom-body β-lobe axonal midline crossing (see Fig. S4*A* for detailed experimental-timeline). The amino acid sequence of CaMK1 is highly conserved between *Homo sapiens*, *Rattus norvegicus*, and *D. melanogaster*, including key residues known to be involved in binding ATP-competitive kinase inhibitors (Fig. 7*A*) (78). In WT *Drosophila*, β-lobe axons are largely excluded from the midline of the mushroom body, but have been observed to have midline crossing defects at frequencies of ~20% (79). However, under conditions that disrupt normal axonal growth, increased frequency of midline crossing is observed for these axons (mild, moderate, and severe). The qualitative scheme for assessing the extent of midline crossing is depicted in Fig. 7*B*, and the frequencies of the different effects of severity are summarized in Fig. 7*C*. We found that 6-OH and PD exposure produced qualitatively similar increases in midline crossing, consistent with the involvements of both CaMK1 and MEK–ERK signaling in axonal growth. More mild effects were observed for BDE-47 and 5-OH-BDE-47 (5-OH) exposures. This became more evident when the distribution of crossing frequencies was rank-scored for each exposure and assessed quantitatively (Fig. 7*D*). Analysis of the rank score revealed that 6-OH and PD shift the median effect from "none" (as in the DMSO control) to "mild," although the parent compound and 5-OH did not produce a significant change. We also found that larval 6-OH exposure led to globally-reduced levels of ERK activation, measured as the fraction of pERK detectable in total ERK immunoprecipitates from larval tissue samples (Fig. S4*B*). These data indicate that 6-OH exposure can dysregulate axonal guidance *in vivo* and that the effect may be mediated via impairment of developmental CaMK1 and MEK–ERK signaling.

Discussion

PBDEs are well-known environmentally-pervasive toxins that are concerning for human health, especially considering the growing body of evidence linking their exposure levels to behavioral abnormalities related to NDDs. Much work has been done characterizing the effects and mechanisms of toxicity of PBDEs, but there is still not a clear general understanding of how these compounds compromise the developing nervous system and how the effects are related to adverse phenotypic outcomes. In this study, we propose a novel mechanistic hypothesis regarding how certain hydroxylated metabolites of common PBDEs (including BDE-47 and BDE-99) exert effects in neurons. We corroborate earlier findings indicating that exposure to an ortho-hydroxylated BDE-47 metabolite, 6-OH, impacts synaptic functionality, and we extend those findings by showing that 6-OH exposure affects neurodevelopmental processes *in vivo*. We also, for the first time, demonstrate that an ortho-hydroxylated PBDE metabolite is a promiscuous kinase inhibitor and that specific metabolites can impair neuronal MEK–ERK signaling.

From our previously published work (38), we had made two predictions related to the effects of chronic 6-OH exposure that are relevant to the data presented here: 1) effects in developing neurons likely manifest at the level of synaptic functionality, and 2) 6-OH may be capable of inhibiting intracellular signaling at or downstream of membrane depolarization and PKC. Primary cortical neuronal cultures grown on MEAs (Figs. 1 and 2) allowed us to directly test the first hypothesis. While some recent studies have begun to employ MEAs to study PBDE developmental neurotoxicity as part of larger screens (80–82), the data presented here are, to our knowledge, the first example of such evidence for hydroxylated PBDE metabolite-induced effects. They demonstrate that chronic nanomolar 6-OH exposures suppress both spontaneous and evoked electrical activity and suggest that the exposures may specifically impact presynapses, including synapsin-related signaling and function. Inhibition of CaMK1 may interfere with neurotransmitter vesicle release by preventing phosphorylation of a well-known presynaptic target, synapsin1–serine 9 (74). This phosphorylation event is known to promote release of sequestered vesicles for exocytosis at the pre-synaptic membrane. Subsequent ERK activation is also known to be involved in recycling of vesicles via further synapsin1 phosphorylation-dependent mechanisms (83, 84). 6-OH–mediated CaMK1 inhibition and subsequent impairment of ERK induction could thus dysregulate pre-synaptic vesicle cycling, potentially explaining the observed effects of 6-OH on spontaneous electrical activity and synapsin protein levels (Fig. 1, *B* and *C*). These pre-synaptic defects and the pronounced effect of 6-OH on evoked activity under the Bic washout treatment paradigm, which has been previously published as a model of *in vitro* plasticity (63), may partially explain the reported relationship between learning deficits and BDE-47/99 exposure in animal studies (9), and it is known that their hydroxylated metabolites can be produced endogenously, primarily via CYP2B6, which is dynamically expressed in the brain (31–33, 85–87).

Figure 4. Acute 6-OH–BDE-47 exposure impairs MEK–ERK signaling. *A, top panel:* synaptosomes were prepared from neurons acutely exposed (20 min pre-treatment) to 5 μM 6-OH with and without Bic + 4AP stimulus (10 min). Levels of the CaMK1 target pSynapsin1(serine 9) were assessed via Western blotting. $n = 2$. *Bottom panel:* to reproduce a previously reported effect linking CaMK1 to MEK–ERK activity (70), neurons were acutely exposed (60 min pre-treatment) to the CaMKK inhibitor STO-609 prior to treatment with Bic + 4AP for 10 min (indicated as +*B10*′). Inhibition of pERK induction was assessed by Western blotting and is quantified below. $n = 3$, p value generated by unpaired one-tailed t test. *B,* cells acutely exposed (20 min pre-treatment) to BDE-47 or one of its hydroxylated metabolites were stimulated with Bic + 4AP for 10 min before collecting whole-cell lysates. Activation of MEK–ERK signaling was assessed by Western blotting, measuring pERK and pMEK levels. Note, the *lower band* in the *MEK panel* is the ERK band visualized on the same blot. Quantification relative to total ERK and MEK is shown below representative blots. $n = 3$–6, p values generated by one-way ANOVA with post hoc LSD. pERK quantification: treatment $F(7,22) = 9.822$, $p < 0.0001$. pMEK quantification: treatment $F(7,16) = 7.805$, $p = 0.0004$. *C,* same experimental design as in *B.*, but neurons were stimulated with TTX + PMA to induce MEK–ERK signaling synapse-independently. $n = 3$. pERK quantification: treatment $F(7,16) = 37.95$, $p < 0.0001$.

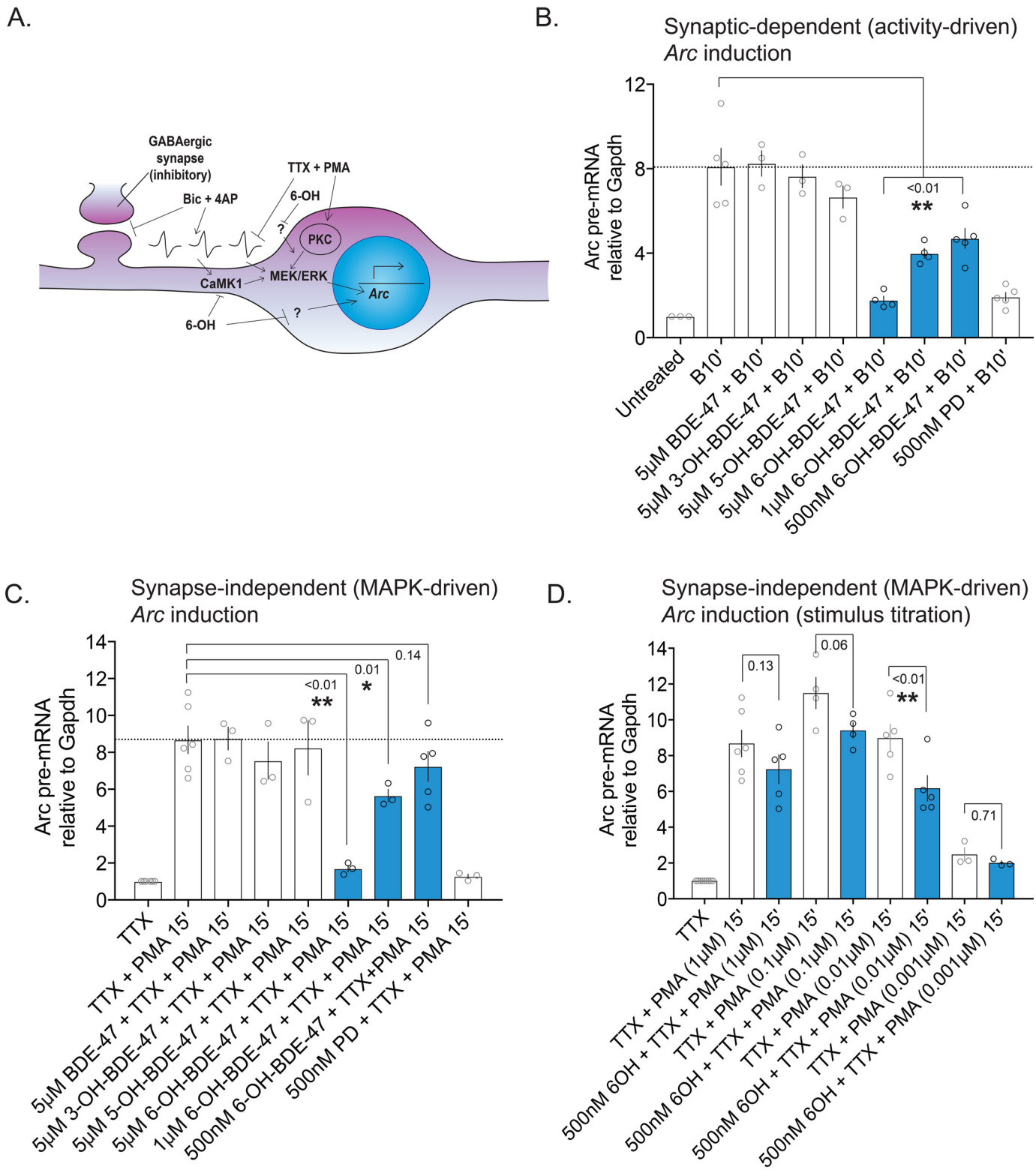

Figure 5. Acute 6-OH–BDE-47 exposure attenuates activity and MEK–ERK-dependent *Arc* transcription. MAPK-dependent gene transcription was evaluated as a measure of 6-OH–mediated MEK–ERK inhibition by quantifying levels of *Arc* pre-mRNA following multiple stimulation approaches. *A,* graphical depiction of the stimulation methods used: Bic + 4AP synaptically activates MEK–ERK signaling via depolarization, whereas TTX + PMA suppresses neuronal activity and activates MEK membrane-independently via PKC. Both ultimately drive induction of *Arc* gene transcription. *B, Arc* pre-mRNA levels were estimated following exposure to BDE-47 or one of its hydroxylated metabolites, and treatment with Bic (50 μM) and 4AP (75 μM), $n = 3–5$, p values generated by one-way ANOVA with post hoc LSD. Treatment $F(7,24) = 25.1$, $p < 0.0001$. *C,* similar to *B,* except that cells were stimulated with TTX (1 μM)) and PMA (1 μM)), $n = 3–6$. Treatment $F(7,21) = 12.14$, $p < 0.0001$. *D,* assessment of the effect of stimulus strength on inhibition of *Arc* induction by 6-OH. Neurons were acutely exposed to 500 nM 6-OH before stimulus with a range of PMA concentrations (1 μM)-1 nM), $n = 3–6$. p values generated by two-way ANOVA with post hoc LSD. PMA-dose: $F(3,27) = 33.16$, $p < 0.0001$; 6-OH exposure: $F(1,27) = 9.969$, $p = 0.0039$; interaction: $F(3,27) = 0.7964$, $p = 0.5066$.

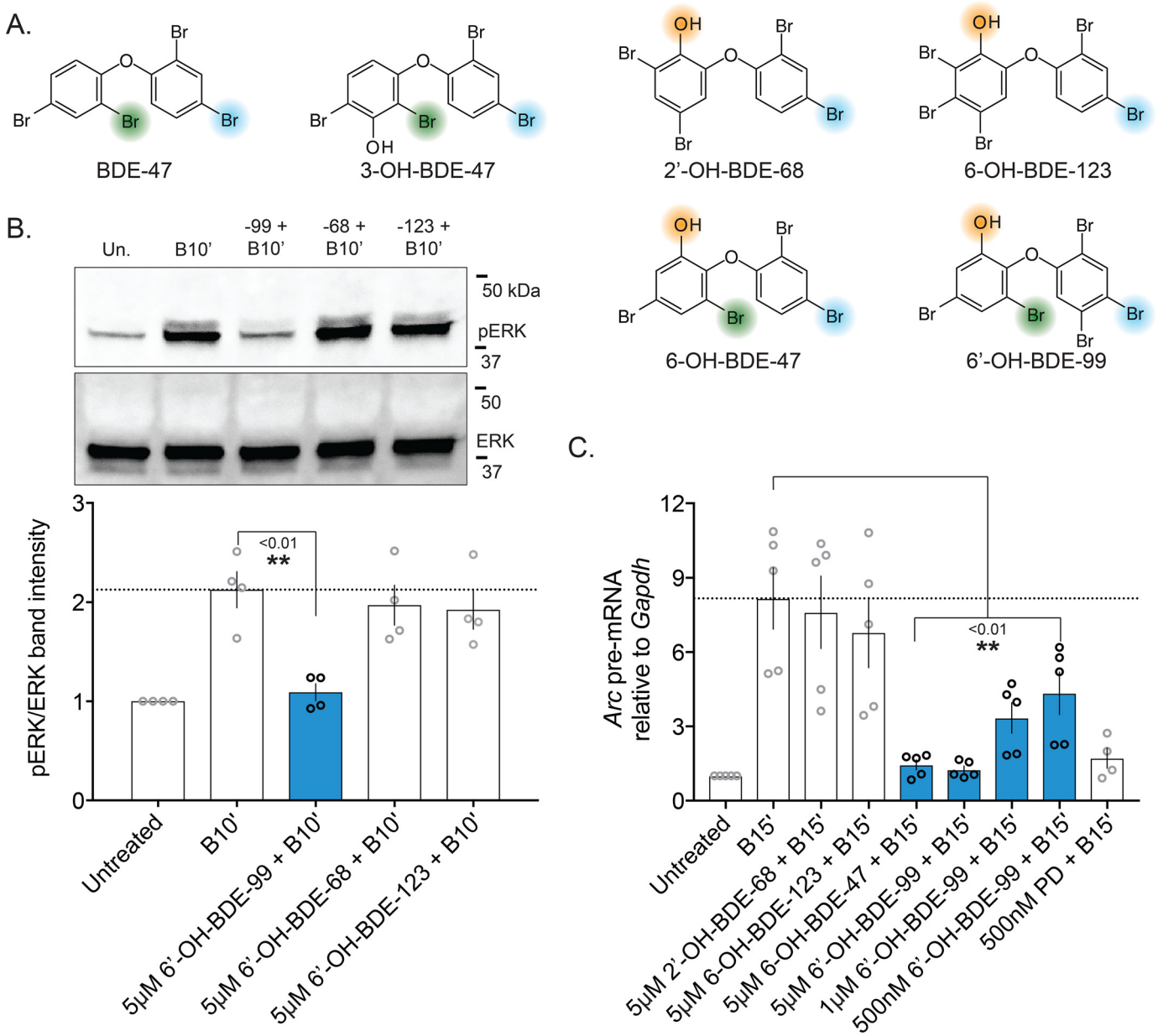

Figure 6. Specific ortho-hydroxylated PBDE metabolites impair neuronal MEK–ERK signaling. In an effort to generalize our hypothesis that ortho-hydroxylated PBDE metabolites can inhibit MEK–ERK signaling, both approaches used to evaluate MEK inhibition by BDE-47 and its metabolites (Figs. 4 and 5) were re-employed with several additional ortho-hydroxylated metabolites. *A,* chemical structures of PBDEs screened, with key substituents for potential MEK1 binding highlighted, specifically indicating the newly-identified ortho-halogen thought to be critical for inhibition of MEK–ERK signaling. *B,* representative Western blotting measuring pERK levels after exposure to various ortho-hydroxylated PBDEs (*top*) with quantification of blots summarized (*bottom*), $n = 4$. p values were generated by one-way ANOVA with post hoc LSD. Treatment: $F(3,12) = 7.314$, $p = 0.0048$. *C,* similar PBDE metabolite exposures as in *B,* but evaluating *Arc* pre-mRNA level attenuation by BDE-47 and BDE-99 metabolites, $n = 4–5$. Treatment: $F(7,31) = 8.837$, $p < 0.0001$.

Investigation of the second prediction generated from our previous work was spurred on by several lines of evidence: our previous observation of disrupted MAPK-driven gene induction by 6-OH (38); the known role of MAPK signaling in the effects seen on Bic-induced neuronal activity (Fig. 2) (63); and the serendipitous observation that 6-OH shares key chemical features with a class of inhibitors designed for MEK1, a central kinase in the MAPK-signaling cascade (61, 88). The structural similarities and results from ligand–protein docking simulations encouraged us to pursue 6-OH as a potential MEK1 inhibitor (Fig. S2*A*). Surprisingly, we came to find that 6-OH does not directly inhibit MEK1/2, but rather it appears to be a promiscuous ATP-competitive kinase inhibitor (Fig. 3). We believe this novel finding will be of use in generating future hypotheses and furthering the understanding of the complicated and diverse effects of the PBDE exposures documented to date. Here, we further pursued effects related to MEK–ERK signaling, particularly related to CaMK1, using multiple approaches to activate the pathway, mediated both synaptically and synapse-independently (Fig. 5*A*). We subsequently found that acute 6-OH exposures impair induction of MEK–ERK signaling and gene transcription (Figs. 4 and 5). Strong inhibition was found with 6-OH concentrations consistent with the data from the kinase screen (Fig. 3), whereas the lower, more environmen-

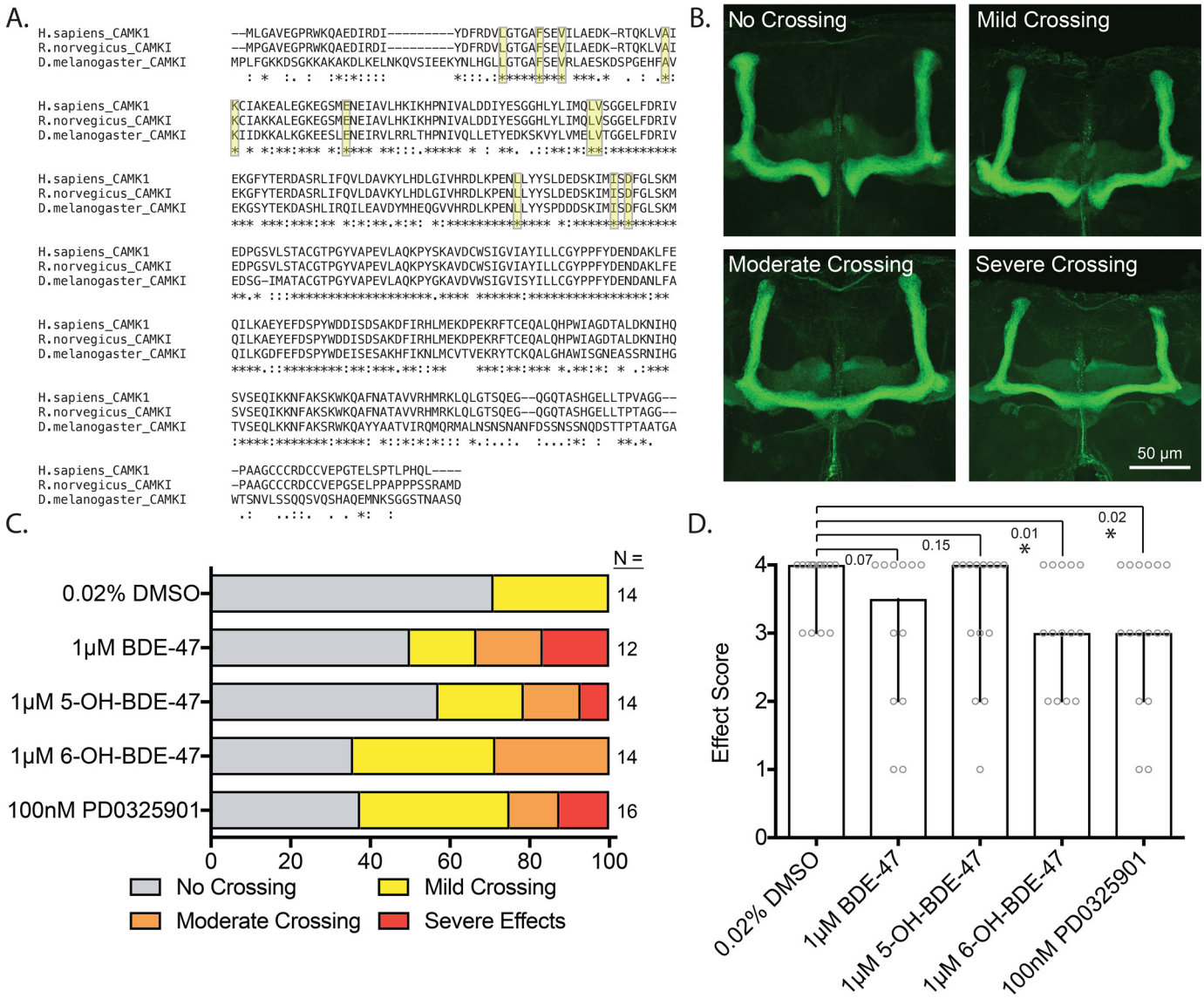

Figure 7. *In vivo* exposure to 6-OH–BDE-47 and the MEK inhibitor PD0325901 disrupt axonal guidance. Canton-S flies (*D. melanogaster*) were exposed to BDE-47, 5-OH, 6-OH, or PD via feeding. The mushroom bodies of offspring were then assessed for aberrant midline crossing. *A,* alignment of the amino acid sequences of human CaMK1 and its rat and fly orthologs. The proteins are highly conserved, including the key residues thought to mediate ATP-competitive inhibitor binding (*highlighted in yellow*). *B,* example images of the effect categories used in the qualitative scoring scheme. *C,* crossing frequency by severity level for each of the treatment groups, $n = 12–16$. *D,* crossing severity was numerically ranked scored as follows. No crossing, 4; mild crossing, 3; moderate crossing, 2; severe crossing and/or lobe malformation, 1. *Bars* represent the median score of each treatment group that was generated from the values of the crossing data from *C,* after application of the numerical scoring scheme (the score for each fly is additionally plotted as *gray circles*). *Error bars* represent 95% confidence intervals. *p* values were generated using exact one-tailed Mann-Whitney tests to compare the median of each group with that of the DMSO control, $n = 12–16$.

tally-relevant doses had milder effects, although still pronounced in the case of *Arc* transcription (Fig. 5). Additionally, we found that time-of-exposure does not appear to increase the extent of inhibition by these lower concentrations of 6-OH (Fig. S3*A*) and that the strength of the stimulus driving MEK–ERK activation affects the extent of 6-OH–mediated impairment, with lighter stimuli leading to stronger impairment for both the synaptic and PMA-driven MEK activation (Fig. S3*C* and Fig. 5*D*). Overall, it is likely that acute exposures to environmentally-relevant levels of MEK-inhibiting ortho-hydroxylated metabolites are not sufficient to widely suppress MEK–ERK signaling throughout the cell (especially given the extensive feedback opposing perturbations), but they may chronically and regionally accumulate to high enough concentrations to inhibit various kinases regulating MEK–ERK signaling in specific subcellular locations, an interesting possibility that is further discussed below.

To generalize our findings, we screened several other ortho-hydroxylated metabolites of BDEs-68/99/123 and found that the metabolite of BDE-99 also impairs MEK–ERK signaling following acute exposure (Fig. 6). While initially surprising, these data indicate that in order for an ortho-hydroxylated PBDE metabolite to be effective at impairing MEK–ERK signaling, it also specifically requires an ortho-substituted halogen that presumably enables binding to susceptible kinases. Taken together, these several lines of molecular evidence demonstrate

that specific ortho-hydroxylated PBDE metabolites can inhibit MEK–ERK signaling *in vitro*. This potential for acute MEK–ERK impairment, combined with chronic exposure–induced deficits in synaptic activity and composition, corroborates and further explains our previous findings concerning the ability of cortical neurons to induce *Arc* expression following chronic 6-OH exposure (38).

To validate our *in silico* and *in vitro* findings and extend them *in vivo*, we compared the exposure effects of 6-OH and PD using a neurodevelopmentally-relevant readout in fruit flies (*D. melanogaster*). *Drosophila* was chosen due to its amenability as an animal model for screening axonal guidance. Importantly, the *Drosophila* ortholog of CaMK1 is highly conserved, including the key amino acid residues that mediate binding of ATP-competitive inhibitors (Fig. 7*A*). Furthermore, it is known that CaMK1 and MEK–ERK signaling plays a role in developmental axon growth (89). One study reported that a let-60c mutation (a *Caenorhabditis elegans* ortholog of KRAS, a membrane GTPase upstream of MEK) led to axonal guidance defects manifested as aberrant ventral midline crossing (52). Another confirmed that MEK–ERK signaling regulates netrin-1–dependent axonal branching in cultured hamster sensorimotor cortical neurons (53). In our studies, exposure was accomplished via oral administration to the P1 generation—to ensure embryonic exposure—and also to F1 larva to cover the neurodevelopmental period of the mushroom-body formation. The brains of offspring were examined post-eclosion to assess the extent of mushroom-body β-lobe axonal midline crossing (see Fig. 4*A* for detailed timeline). Here, we found that 6-OH and PD exposures produced qualitatively similar increases in midline crossing, with BDE-47 and 5-OH also increasing crossing frequency, but to a lesser extent (Fig. 7*C*). After applying a numerical scoring scheme and quantifying the effects, we found that 6-OH and PD shift the median effect to "mild," whereas the parent compound and 5-OH did not produce a significant change. These data represent an *in vivo* confirmation of the effects of 6-OH exposure on axonal guidance (previously reported in primary hippocampal cultures (90)) and indicate that the effect may be mediated by disruptions to CaMK1 and MEK–ERK signaling. These findings align well with previous reports in *C. elegans*, where mutants of let-c, an ortholog of an upstream MAPK-signaling component, KRAS, exhibit aberrant axonal crossing of the ventral midline (52).

Although the evidence we present here demonstrates the promiscuous inhibitory potential of ortho-hydroxylated metabolites toward ATP-dependent kinases and MEK–ERK signaling, we note that such effects are highly nuanced and will require further investigation. MEK–ERK signaling is activated by a variety of stimuli in neurons and is a very dynamic process. Here alone we have identified CaMK1 and DYRK3 disruption as potential avenues of MEK–ERK impairment. Known modulation of Ca^{2+} homeostasis by 6-OH further complicates interpretation of acute exposures and potentially explains the inhibition of pERK levels by 6-OH following the synapse-independent stimulus paradigm (Fig. 4*C*). Further examples of nuanced effects include cultures chronically exposed to 500 nM 6-OH were able to synaptically induce cytosolic pERK to the same extent as untreated controls, while significantly less pERK was available in the nucleus (Fig. S3, *B* and *C*). This was unexpected, especially given the compromised electrical activity observed for chronically-treated cells, but could be explained by the extensive homeostatic feedback mechanisms known to regulate MEK–ERK signaling (91). Such feedback mechanisms may also explain the discrepancy between our findings and those of another recent report that showed that exposures to 6-OH selectively impaired ERK5 phosphorylation, but not ERK1/2, in adult neural stem cells (aNSCs) (92). In this study, the authors incubated aNSCs overnight with 5 μM 6-OH, followed by a stimulus with epidermal growth factor/basic fibroblast growth factor to induced MAPK, and they reported no decrease in the amount of pERK1/2. In addition to the data from this study showing that after prolonged treatment with 6-OH the cortical neurons induce the same level of pERK as untreated controls, it has been shown in mouse embryonic stem cells that acute PD treatment reduces pERK levels, but between 12 and 24 h later, the pERK signal strongly returns (93). Therefore, it is possible that either feedback within the MAPK pathways or differences in signaling dynamics in aNSCs, particularly those that activate MEK–ERK signaling, account for this discrepancy between our observation and that by Li *et al.* (92).

Interestingly, chronic 6-OH treatment-induced differences in cytosolic and nuclear pERK inhibition also suggest another nuanced aspect of PBDE toxicity: their subcellular localization and localized effects. Because of the highly-lipophilic nature of PBDEs, they are likely to be more concentrated within close proximity of lipid membranes. Supporting this notion, it has been demonstrated that several PBDEs localize in higher amounts in mitochondrial and microsomal fractions collected from cerebral granule neurons (94). Accordingly, it will be interesting and necessary to evaluate the potential of ortho-hydroxylated PBDE metabolites to inhibit kinases in specific subcellular locations, as well as MEK–ERK signaling events, which are also known to be localized in different cellular compartments, including the cytosol, mitochondria, outgrowing neurites, and synapses (95, 96). Considering the effects on such compartmentalized signaling, inhibition may help to generally explain some of the various documented effects of exposure to certain PBDEs, especially well-documented mitochondrial toxicity (21). Furthermore, mitochondrial toxicity may link PBDE exposure to NDD etiology given the known comorbidity of mitochondrial deficits and autism (12). Pre-synaptic accumulation could also be involved in the strong effect seen on synapsin (Figs. 1*C* and 4*A*), as it and other synaptic proteins are known targets of CaMK1 and synapse-localized MAPKs (97, 98). Both CaMK- and MAPK-dependent synapsin phosphorylation are also known to play a role in pre-synaptic plasticity (59, 74, 84, 99). Local inhibition of CaMK1 and MAPK signaling and subsequent impairment of pre-synaptic vesicle regulation may explain the suppressed electrical activity caused by chronic 6-OH exposure (Figs. 1 and 2), although more work is needed for confirmation.

Taken together, the findings presented here provide new evidence on the effects of exposure to hydroxylated PBDE metabolites and establish novel insight into the underlying molecular mechanisms that mediate their toxicity. The indication that

PBDE metabolites are capable of impairing MEK–ERK signaling sets up several potential avenues for further investigation. One takes into account another aspect of our previously published work (38), *i.e.* 6-OH exposure dysregulates expression of BAF chromatin remodeling subunits. This evidence, along with a recent preprint report concerning ERK1/2 regulation of neurodevelopmental polycomb-repressive complex chromatin remodeling that further speculates about additional regulation of BAF complex composition (100), suggests that 6-OH exposure may interact with chromatin remodeling via modulation of MAPK signaling. More closely related to this study, it will be critical to investigate the role of ortho-hydroxylated PBDEs as promiscuous kinase inhibitors, their links to impairment of MEK–ERK signaling, and the many established routes of PBDE toxicity. This will be especially interesting for effects related to mitochondrial function, calcium homeostasis, and regulation of synaptic function. Overall, such future studies may help to clarify the growing evidence linking human PBDE exposures to NDDs and perhaps provide useful insight into these challenging disorders.

Materials and methods

Primary neuronal culture and cell treatment

Timed-pregnant Sprague-Dawley rats were obtained from Charles River Laboratories. Dams were consistently delivered 2 days prior to dissection and housed individually on a 12-h light/dark cycle with access to food and water *ad libitum*. On the day of dissection, dams were anesthetized with Euthasol® euthanasia solution (pentobarbital 390 mg/ml, phenytoin 50 mg/ml) in order to minimize distress. Loss of responsiveness was ensured with the toe pinch method, confirming a lack of reflex prior to decapitation via guillotine. Primary cultures of cortical neurons were then prepared from embryonic day 18 pups (IACUC approval, AUP 16-0004, University of California, Merced). Cortical hemispheres were isolated and pooled from male and female embryos in magnesium- and calcium-containing HBSS (Gibco, catalog no. 14025092). They were then mechanically dissociated by pipetting with a fire-polished Pasteur pipette following a 7-min digestion with StemPro® Accutase® (Life Technologies, Inc., catalog no. A1110501). The enzyme was then deactivated by diluting the triturated cell suspension in HBSS lacking calcium and magnesium (Gibco, catalog no. 14175095). The dissociated cortical neurons were then pelleted by centrifugation, resuspended in plating media, counted using trypan blue and a TC20™ automated cell counter (Bio-Rad, catalog no. 1450102), and subsequently plated by addition to dishes containing pre-warmed Neurobasal medium (Gibco, catalog no. 21103049) supplemented with 25 μM glutamate (Sigma-Aldrich, catalog no. 1446600), 0.5 mM L-glutamine (Sigma-Aldrich, catalog no. G8540), and 2% NS21 supplement. Cells were maintained at 37 °C in a humidified incubator with 5% CO_2. They were grown in the medium described above without glutamate, replacing half the media every 3–4 days. NS21 was prepared in the laboratory as described previously (101). Neurons were used for various assays between 10 and 14 days *in vitro*. No blinding was performed for experiments from cultured cells. To induce MEK–ERK signaling and gene transcription using synaptic activity, neurons were co-treated with 50 or 5 μM bicuculline (Sigma-Aldrich, catalog no. 14340) with or without 75 μM 4-aminopyridine (Acros Organics, catalog no. 104571000). To induce gene transcription synapse independently, membrane activity was blocked with 1 μM TTX (Calbiochem, catalog no. 554412), and the MAPK pathways were activated via PKC with 1 μM to 1 nM phorbol 12-myristate 13-acetate (PMA; Sigma-Aldrich, catalog no. P1585). BDE-47 and hydroxylated BDE metabolites used to treat cultures were obtained from AccuStandard (BDE-047N, HBDE-4003N, HBDE-4004N, HBDE-4005N, HBDE-4006N, HBDE-5006-N, and HBDE-5011N) and initially dissolved in dimethyl sulfoxide (DMSO) at 2 and 5 mM stock concentrations. Final treatment concentrations were produced at the time of treatment by dilution in culture medium. PD0325901 was obtained from AdipoGen (SYN-1059), dissolved in DMSO at 5 mM, and similarly diluted at the time of treatment.

Microelectrode array recording and data processing

Neurons from the preparations described above were plated on poly-L-lysine/laminin–coated MEAs (60MEA200/30-Ti, MultiChannel Systems (MCS), Reutlingen, Germany) in 500 μl of the NS21-supplemented Neurobasal plating medium described above. When cells were fed, again every 3–4 days, approximately half the media was replaced with NS21-supplemented BrainPhys feeding media (StemCell). This was done to promote optimal conditions for neuronal firing, which has been shown to be enhanced in BrainPhys media (102). Recordings were made with an MEA2100-lite system that interfaces with MCS provided MultiChannel Experimenter software. Sampling was conducted at 10–20 kHz in 3-min sessions at room temperature (arrays were covered to prevent contamination). Recording were post-processed in a MultiChannel Analyzer with a high-pass 1st order Butterworth filter with 100 Hz cutoff prior to generation of spike time-stamps. Spikes were detected by an automatic threshold estimator set to 6–8 standard deviations from the baseline signal. To quantify burst properties, the MultiChannel Analyzer burst detection tool was used with the following settings: maximum interval to start burst, 25 ms; maximum interval to end burst, 250 ms; minimum interval between bursts, 1500 ms; minimum duration of burst, 50 ms; minimum number of spikes in burst, 5. Raster images from example recordings were generated in NeuroExplorer (RRID:SCR_001818, NexTechnologies, Herndon, VA).

Ligand–protein docking simulations

For ligand–protein docking simulations, we used AutoDock Vina (RRID:SCR_011958), an open-source molecular docking program made available through the Scripps Research Institute (66). Initially, blind-docking of 6-OH–BDE-47 and PD0325901 was conducted with large areas of a published crystal structure of human MEK1 (PDB code 3EQI (103)). Subsequent simulations searching a smaller grid-space centered around the catalytic binding domain were then conducted. Several of the top hits from the kinase inhibition screen reported here were also used in docking simulations with 6-OH–BDE-47: CAMK1 (4FG7 and 4FGB (104)); DYRK3 (5Y86 (78)); HIPK2 (6P5S (105)); MAPKAP-K3 (3R1N (106)); and PIM1 (1YXT (107)).

The simulations were run with standard parameters for a rigid receptor and ligands with rotatable bonds (108). The binding structures were evaluated visually based on comparison with the well-characterized binding modes of allosteric MEK inhibitors, the first example of which was published in 2004 (109), as well as with various ATP-competitive kinase inhibitors crystallized with some the of the other kinases.

Western blotting, imaging, and antibodies

Neurons were lysed in ice-cold 1× RIPA buffer (25 mM Tris-HCl, pH 7.5, 150 mM NaCl, 1% Na-deoxycholate, 0.1% SDS, 0.1% NP-40) supplemented with 1:100 protease/phosphatase inhibitor mixture (Thermo Fisher Scientific, catalog no. 78442). Nuclear lysates were prepared by first washing cells with ice-cold 1× PBS, applying Plasma Membrane Lysis Buffer (PMLB) (25 mM Tris-HCl, pH 7.6, 10 mM KCl, 1.5 mM $MgCl_2$, 0.5 mM DTT, 0.1% NP-40) for 1 min on ice, washing with PMLB, and then collecting in 1× RIPA buffer, pH 7.4. Lysates were sheared by sonication (low setting; three cycles on Bioruptor®); cell debris was pelleted at 15,000 rpm for 5 min at 4 °C, and clarified supernatant was transferred to a pre-chilled 1.5-ml microcentrifuge tube. Synaptosomal isolations were prepared using Syn-PER according to manufacturer's instructions (Thermo Fisher Scientific, catalog no. 87793). The various cell extracts were denatured at 95 °C for 5 min, using either 2× or 4× Laemmli sample buffer (Bio-Rad, catalog nos. 1610737 and 1610747). Denatured protein samples were resolved on 4–20% (Bio-Rad, catalog no. 4568095) or 4–15% (Bio-Rad catalog no. 456–1083) mini PROTEAN® gels in Tris/glycine/SDS (Bio-Rad catalog no. 1610772). Resolved proteins were transferred onto PVDF membrane, using the Bio-Rad TBT RTA kit and protocol using either 10% MeOH- or 20% EtOH-containing transfer buffer (catalog no. 1704272). PVDF membranes were incubated at 4 °C overnight with appropriate primary antibodies in 1× TBS-T with 1.5% BSA. Primary antibodies included the following antibodies: β-actin (Thermo Fisher Scientific, catalog no. AM4302, RRID:AB_2536382); H4 (CST catalog no. 2935, RRID:AB_1147658); pERK (CST catalog no. 4370, RRID:AB_2315112); ERK (CST catalog no. 4696, RRID:AB_390780); pMEK (CST catalog no. 9154, RRID:AB_2138017); MEK (CST catalog no. 2352, RRID:AB_10693788); synapsin1 (SySy catalog no. 106011, RRID:AB_2619772);PSD-95 (NeuroMab catalog no. 75-028, RRID:AB_2292909); gephyrin (SySy catalog no. 147111, RRID:AB_887719); synaptotagmin6 (NeuroMab catalog no. 75-271, RRID:AB_11001830); and synaptophysin1(SySy catalog no. 101011, RRID:AB_887824). The next day, membranes were washed three times in 1× TBST for 5 min each, probed with either goat anti-mouse-647 (RRID:AB_2535808) or goat anti-rabbit-546 Alexa Fluor (RRID:AB_2534093) secondary antibodies (Life Technologies, Inc.) for 45 min at room temperature, washed three times with 1× TBS-T for 5 min each, and imaged using Bio-Rad Multiplex ChemiDoc™ Imaging System.

RNA extraction and gene transcription quantitation

Total RNA was isolated from cultured neurons using the Illustra RNAspin mini kit (GE Healthcare, catalog no. 25050072). Specific pre-mRNAs from these total RNA samples were initially amplified by cDNA synthesis (14 cycles) using Arc and Gapdh primers overlapping an intron–exon junction and a OneStep RT-PCR kit (Qiagen, catalog no. 210212). Quantitative real-time PCR was then performed from this cDNA to quantify levels of specific transcripts using PerfeCTa SYBR Green FastMix (QuantaBio, catalog no. 95072-012) and the Bio-Rad CFX Connect real-time PCR detection system. Fold-change from control was estimated using the $\Delta\Delta Ct$ method.

Drosophila rearing and chemical exposure

WT Canton-S *Drosophila* were maintained at 25 °C in a humidified incubator on a standard cornmeal diet (Bloomington *Drosophila* Stock Center standard cornmeal medium). No randomization was performed to allocate individuals in the various treatment groups. For oral administration of PD0325901, BDE-47, 5-OH, and 6-OH, compounds were dissolved in dimethyl sulfoxide (DMSO) and then added directly to warm food, prior to solidification. The concentration of DMSO was maintained at 0.02% for all exposures. *Drosophila* were exposed to PD ($n = 16$) at a concentration of 100 nM. For all other chemicals (BDE-47 ($n = 12$), 5-OH ($n = 14$), and 6-OH ($n = 14$)), *Drosophila* were exposed to a concentration of 1 μM. Control flies were exposed to DMSO alone ($n = 14$).

Fluorescence labeling and microscopy of Drosophila whole-mount brain preparations

Whole-mount immunostaining of adult male brains (0–2 days old) was performed as described previously (79), except that brains were fixed for 25 min in 4% paraformaldehyde. Anti-Fasciclin II (RRID:AB_528235) was used at a 1:20 dilution. Alexa Fluor 488–conjugated goat anti-mouse secondary (RRID:AB_2338840) was used at a 1:1000 dilution. Images were captured using an Olympus laser-scanning confocal microscope. Separate individuals, who were blinded to the exposure group and file-naming system, assessed the images for phenotypic scoring.

Immunoprecipitations (IPs) from Drosophila larval tissue

IPs were conducted by pooling the heads from 10 chemically-exposed larvae. Tissue was lysed in ice-cold 1× RIPA buffer (25 mM Tris-HCl, pH 7.5, 150 mM NaCl, 1% Na-deoxycholate, 0.1% SDS, 0.1% NP-40) supplemented with 1:100 protease/phosphatase inhibitor mixture (Thermo Fisher Scientific, catalog no. 78442). Lysate was added to a total volume of 1 ml in IP buffer (0.5% Triton X-100, 2 mM EDTA, 0.02 M Tris, pH 7.75, 150 mM NaCl, and 10% glycerol) with 4 μg of total ERK antibody (CST, catalog no. 4696, RRID:AB_390780) and rotated for 2 h at room temperature. Protein A/G magnetic beads (Thermo Fisher Scientific, catalog no. 88803) were then added to the IPs, followed by rotation at room temperature for 1 h. IPs were then washed three times on a magnetic rack with 1 ml of wash buffer (0.5% Triton X-100, 2 mM EDTA, 0.02 M Tris, pH 7.75, 150 mM NaCl, 10% SDS), resuspending the magnetic beads between each wash. After the final wash, the isolated proteins were denatured at 95 °C for 5 min prior to gel electrophoresis and Western blotting by the procedure described under "Western blotting, imaging, and antibodies."

Study design and statistical analysis

This study was not pre-registered. Data presented were generated from both hypothesis-confirming and exploratory experiments. For rat primary culture experiments, no sample size calculation was performed. For *Drosophila* experiments, sample size was estimated based on previously published studies that have examined the mushroom-body phenotype (79). There were no pre-determined exclusion criteria for animal work. Statistical analyses were conducted using GraphPad Prism 7 (RRID:SCR_002798, GraphPad software, San Diego, CA). Error bars represent standard error of the mean throughout, except in Fig. 7*D* where they represent 95% confidence intervals. Data were assessed for normality with the Shapiro-Wilk normality test. No tests for outliers were conducted; therefore all data points were included. Effects were determined by *t* test or one-/two-way ANOVA with appropriate post hoc tests for generation of specific *p* values; details are indicated in the figure legends. The only exception is Fig. 7*D* where the nonparametric Mann-Whitney *U* test was used to compare the medians of effect score distributions for the various treatment groups. Specific *p* values are indicated on the figures: * indicates *p* value <0.05 and ** indicates *p* value <0.01 throughout. Biological replicates are indicated throughout as *N* in corresponding figure legends. Biological replicates constitute cell culture preparations from the pooled cortices of embryos from independent litters or brains of individual flies.

Data availability

All data are included in the text. Raw datasets are available upon request.

Author contributions—R. G. P. and R. N. S. conceptualization; R. G. P., L. M., A. R., M. G.-E., and J. S. data curation; R. G. P., L. M., A. R., M. G.-E., and J. S. formal analysis; R. G. P. and R. N. S. validation; R. G. P., A. R., M. G.-E., J. S., and R. N. S. investigation; R. G. P. and R. N. S. visualization; R. G. P., K. M., and R. N. S. methodology; R. G. P. and R. N. S. writing-original draft; K. M. and R. N. S. resources; K. M. and R. N. S. supervision; K. M. and R. N. S. funding acquisition; R. N. S. project administration; R. N. S. writing-review and editing.

Acknowledgments—We thank all Saha Lab members for their support and constructive criticism during experimentation and manuscript preparation. We thank Alex Ceballos, Daniel Chu, Kaitlin Danziger, Jomari Gabriel, and Chloe Welch for technical assistance and Dr. Michael Colvin for sharing his expertise in the in silico component of this manuscript.

References

1. Frederiksen, M., Vorkamp, K., Thomsen, M., and Knudsen, L. E. (2009) Human internal and external exposure to PBDEs–a review of levels and sources. *Int. J. Hyg. Environ. Health* **212,** 109–134 CrossRef Medline
2. Bramwell, L., Glinianaia, S. V., Rankin, J., Rose, M., Fernandes, A., Harrad, S., and Pless-Mulolli, T. (2016) Associations between human exposure to polybrominated diphenyl ether flame retardants via diet and indoor dust, and internal dose: a systematic review. *Environ. Int.* **92,** 680–694 CrossRef Medline
3. Linares, V., Bellés, M., and Domingo, J. L. (2015) Human exposure to PBDE and critical evaluation of health hazards. *Arch. Toxicol.* **89,** 335–356 CrossRef Medline
4. United States Environmental Protection Agency (2010) An exposure assessment of polybrominated diphenyl ethers (PBDE) (final). United States Environmental Protection Agency, Washington, D.C., EPA/600/R-08/086F
5. Grandjean, P., and Landrigan, P. J. (2014) Neurobehavioural effects of developmental toxicity. *Lancet Neurol.* **13,** 330–338 CrossRef Medline
6. Vuong, A. M., Yolton, K., Dietrich, K. N., Braun, J. M., Lanphear, B. P., and Chen, A. (2018) Exposure to polybrominated diphenyl ethers (PBDEs) and child behavior: current findings and future directions. *Horm. Behav.* **101,** 94–104 CrossRef Medline
7. Lam, J., Lanphear, B. P., Bellinger, D., Axelrad, D. A., McPartland, J., Sutton, P., Davidson, L., Daniels, N., Sen, S., and Woodruff, T. J. (2017) Developmental PBDE exposure and IQ/ADHD in childhood: a systematic review and meta-analysis. *Environ. Health Perspect.* **125,** 86001 CrossRef Medline
8. National Academies of Sciences, Engineering, and Medicine (2017) *Application of Systematic Review Methods in an Overall Strategy for Evaluating Low-dose Toxicity from Endocrine Active Chemicals*, The National Academies Press, Washington, D. C.
9. Dorman, D. C., Chiu, W., Hales, B. F., Hauser, R., Johnson, K. J., Mantus, E., Martel, S., Robinson, K. A., Rooney, A. A., Rudel, R., Sathyanarayana, S., Schantz, S. L., and Waters, K. M. (2018) Polybrominated diphenyl ether (PBDE) neurotoxicity: a systematic review and meta-analysis of animal evidence. *J. Toxicol. Environ. Health. B Crit. Rev.* **21,** 269–289 CrossRef Medline
10. Ye, B. S., Leung, A. O. W., and Wong, M. H. (2017) The association of environmental toxicants and autism spectrum disorders in children. *Environ. Pollut.* **227,** 234–242 CrossRef Medline
11. Hertz-Picciotto, I., Bergman, A., Fängström, B., Rose, M., Krakowiak, P., Pessah, I., Hansen, R., and Bennett, D. H. (2011) Polybrominated diphenyl ethers in relation to autism and developmental delay: a case-control study. *Environ. Health* **10,** 1 CrossRef Medline
12. Wong, S., and Giulivi, C. (2016) Autism, mitochondria and polybrominated diphenyl ether exposure. *CNS Neurol. Disord. Drug Targets* **15,** 614–623 CrossRef Medline
13. Messer, A. (2010) Mini-review: polybrominated diphenyl ether (PBDE) flame retardants as potential autism risk factors. *Physiol. Behav.* **100,** 245–249 CrossRef Medline
14. Mitchell, M. M., Woods, R., Chi, L.-H., Schmidt, R. J., Pessah, I. N., Kostyniak, P. J., and LaSalle, J. M. (2012) Levels of select PCB and PBDE congeners in human postmortem brain reveal possible environmental involvement in 15q11-q13 duplication autism spectrum disorder. *Environ. Mol. Mutagen.* **53,** 589–598 CrossRef Medline
15. Woods, R., Vallero, R. O., Golub, M. S., Suarez, J. K., Ta, T. A., Yasui, D. H., Chi, L. H., Kostyniak, P. J., Pessah, I. N., Berman, R. F., and LaSalle, J. M. (2012) Long-lived epigenetic interactions between perinatal PBDE exposure and Mecp2308 mutation. *Hum. Mol. Genet.* **21,** 2399–2411 CrossRef Medline
16. Braun, J. M., Kalkbrenner, A. E., Just, A. C., Yolton, K., Calafat, A. M., Sjödin, A., Hauser, R., Webster, G. M., Chen, A., and Lanphear, B. P. (2014) Gestational exposure to endocrine-disrupting chemicals and reciprocal social, repetitive, and stereotypic behaviors in 4-and 5-year-old children: the HOME study. *Environ. Health Perspect.* **122,** 513–520 CrossRef Medline
17. Napoli, E., Hung, C., Wong, S., and Giulivi, C. (2013) Toxicity of the flame-retardant BDE-49 on brain mitochondria and neuronal progenitor striatal cells enhanced by a PTEN-deficient background. *Toxicol. Sci.* **132,** 196–210 CrossRef Medline
18. Trasande, L., Zoeller, R. T., Hass, U., Kortenkamp, A., Grandjean, P., Myers, J. P., DiGangi, J., Bellanger, M., Hauser, R., Legler, J., Skakkebaek, N. E., and Heindel, J. J. (2015) Estimating burden and disease costs of exposure to endocrine-disrupting chemicals in the European Union. *J. Clin. Endocrinol. Metab.* **100,** 1245–1255 CrossRef Medline
19. Lyall, K., Croen, L. A., Weiss, L. A., Kharrazi, M., Traglia, M., Delorenze, G. N., and Windham, G. C. (2017) Prenatal serum concentrations of brominated flame retardants and autism spectrum disorder and intellectual disability in the early markers of autism study: a population-based case–control study in California. *Environ. Health Perspect.* **125,** 087023 CrossRef Medline

20. Traglia, M., Croen, L. A., Lyall, K., Windham, G. C., Kharrazi, M., DeLorenze, G. N., Torres, A. R., and Weiss, L. A. (2017) Independent maternal and fetal genetic effects on midgestational circulating levels of environmental pollutants. *G3* **7,** 1287–1299 CrossRef Medline
21. Costa, L. G., de Laat, R., Tagliaferri, S., and Pellacani, C. (2014) A mechanistic view of polybrominated diphenyl ether (PBDE) developmental neurotoxicity. *Toxicol. Lett.* **230,** 282–294 CrossRef Medline
22. Sueyoshi, T., Li, L., Wang, H., Moore, R., Kodavanti, P. R., Lehmler, H. J., Negishi, M., and Birnbaum, L. S. (2014) Flame retardant BDE-47 effectively activates nuclear receptor CAR in human primary hepatocytes. *Toxicol. Sci.* **137,** 292–302 CrossRef Medline
23. Pacyniak, E. K., Cheng, X., Cunningham, M. L., Crofton, K., Klaassen, C. D., and Guo, G. L. (2007) The flame retardants, polybrominated diphenyl ethers, are pregnane X receptor activators. *Toxicol. Sci.* **97,** 94–102 CrossRef Medline
24. Wahl, M., Guenther, R., Yang, L., Bergman, A., Straehle, U., Strack, S., and Weiss, C. (2010) Polybrominated diphenyl ethers and arylhydrocarbon receptor agonists: different toxicity and target gene expression. *Toxicol. Lett.* **198,** 119–126 CrossRef Medline
25. Dingemans, M. M., van den Berg, M., and Westerink, R. H. (2011) Neurotoxicity of brominated flame retardants: (In)direct effects of parent and hydroxylated polybrominated diphenyl ethers on the (Developing) nervous system. *Environ. Health Perspect.* **119,** 900–907 CrossRef Medline
26. Bussau, L. J., Beveridge, A. A., Nadeson, R., and Anderson, A. P. (1993) The marine natural product 3,5-dibromo-2-(2,4-dibromophenoxy)phenol, inhibits contractile activity in the guinea pig ileum. *Clin. Exp. Pharmacol. Physiol.* **20,** 697–704 CrossRef Medline
27. Dingemans, M. M., de Groot, A., van Kleef, R. G., Bergman, A., Berg, M. van den Berg, M., Vijverberg, H. P., and Westerink, R. H. (2008) Hydroxylation increases the neurotoxic potential of BDE-47 to affect exocytosis and calcium homeostasis in PC12 cells. *Environ. Health Perspect.* **116,** 637–643 CrossRef Medline
28. Gassmann, K., Schreiber, T., Dingemans, M. M., Krause, G., Roderigo, C., Giersiefer, S., Schuwald, J., Moors, M., Unfried, K., Bergman, Å., Westerink, R. H., Rose, C. R., and Fritsche, E. (2014) BDE-47 and 6-OH–BDE-47 modulate calcium homeostasis in primary fetal human neural progenitor cells via ryanodine receptor-independent mechanisms. *Arch. Toxicol.* **88,** 1537–1548 CrossRef Medline
29. van Boxtel, A. L., Kamstra, J. H., Cenijn, P. H., Pieterse, B., Wagner, J. M., Antink, M., Krab, K., van der Burg, B., Marsh, G., Brouwer, A., and Legler, J. (2008) Microarray analysis reveals a mechanism of phenolic polybrominated diphenylether toxicity in zebrafish. *Environ. Sci. Technol.* **42,** 1773–1779 CrossRef Medline
30. Poston, R. G., and Saha, R. N. (2019) Epigenetic effects of polybrominated diphenyl ethers on human health. *Int. J. Environ. Res. Public Health* **16,** E2703 CrossRef Medline
31. Feo, M. L., Gross, M. S., McGarrigle, B. P., Eljarrat, E., Barceló, D., Aga, D. S., and Olson, J. R. (2013) Biotransformation of BDE-47 to potentially toxic metabolites is predominantly mediated by human CYP2B6. *Environ. Health Perspect.* **121,** 440–446 CrossRef Medline
32. Erratico, C. A., Szeitz, A., and Bandiera, S. M. (2013) Biotransformation of 2,2′,4,4′-Tetrabromodiphenyl ether (BDE-47) by human liver microsomes: identification of cytochrome P450 2B6 as the major enzyme involved. *Chem. Res. Toxicol.* **26,** 721–731 CrossRef Medline
33. Fu, Z., Wang, Y., Chen, J., Wang, Z., and Wang, X. (2016) How PBDEs are transformed into dihydroxylated and dioxin metabolites catalyzed by the active center of cytochrome P450s: a DFT study. *Environ. Sci. Technol.* **50,** 8155–8163 CrossRef Medline
34. Agarwal, V., El Gamal, A. A., Yamanaka, K., Poth, D., Kersten, R. D., Schorn, M., Allen, E. E., and Moore, B. S. (2014) Biosynthesis of polybrominated aromatic organic compounds by marine bacteria. *Nat. Chem. Biol.* **10,** 640–647 CrossRef Medline
35. Agarwal, V., Blanton, J. M., Podell, S., Taton, A., Schorn, M. A., Busch, J., Lin, Z., Schmidt, E. W., Jensen, P. R., Paul, V. J., Biggs, J. S., Golden, J. W., Allen, E. E., and Moore, B. S. (2017) Metagenomic discovery of polybrominated diphenyl ether biosynthesis by marine sponges. *Nat. Chem. Biol.* **13,** 537–543 CrossRef Medline
36. Malmvärn, A., Marsh, G., Kautsky, L., Athanasiadou, M., Bergman, A., Asplund, L. (2005) Hydroxylated and methoxylated brominated diphenyl ethers in the red algae ceramium tenuicorne and blue mussels from the Baltic Sea. *Environ. Sci. Technol.* **39,** 2990–2997 CrossRef Medline
37. Malmvärn, A., Zebühr, Y., Kautsky, L., Bergman, K., and Asplund, L. (2008) Hydroxylated and methoxylated polybrominated diphenyl ethers and polybrominated dibenzo-*p*-dioxins in red alga and cyanobacteria living in the Baltic Sea. *Chemosphere.* **72,** 910–916 CrossRef Medline
38. Poston, R. G., Dunn, C. J., Sarkar, P., and Saha, R. N. (2018) Persistent 6-OH–BDE-47 exposure impairs functional neuronal maturation and alters expression of neurodevelopmentally-relevant chromatin remodelers. *Environ. Epigenet.* **4,** dvx020 CrossRef Medline
39. Spitzer, N. C. (2006) Electrical activity in early neuronal development. *Nature* **444,** 707–712 CrossRef Medline
40. Thomas, G. M., and Huganir, R. L. (2004) MAPK cascade signalling and synaptic plasticity. *Nat. Rev. Neurosci.* **5,** 173–183 CrossRef Medline
41. Tyssowski, K. M., DeStefino, N. R., Cho, J.-H., Dunn, C. J., Poston, R. G., Carty, C. E., Jones, R. D., Chang, S. M., Romeo, P., Wurzelmann, M. K., Ward, J. M., Andermann, M. L., Saha, R. N., Dudek, S. M., and Gray, J. M. (2018) Different neuronal activity patterns induce different gene expression programs. *Neuron* **98,** 530–546.e11 CrossRef Medline
42. Pérez, J., Castañeda-García, A., Jenke-Kodama, H., Müller, R., and Muñoz-Dorado, J. (2008) Eukaryotic-like protein kinases in the prokaryotes and the myxobacterial kinome. *Proc. Natl. Acad. Sci. U.S.A.* **105,** 15950–15955 CrossRef Medline
43. Pereira, S. F., Goss, L., and Dworkin, J. (2011) Eukaryote-like serine/threonine kinases and phosphatases in bacteria. *Microbiol. Mol. Biol. Rev.* **75,** 192–212 CrossRef Medline
44. Widmann, C., Gibson, S., Jarpe, M. B., and Johnson, G. L. (1999) Mitogen-activated protein kinase: conservation of a three-kinase module from yeast to human. *Physiol. Rev.* **79,** 143–180 CrossRef Medline
45. Sharma, G. M., and Burkholder, P. R. (1967) Studies on the antimicrobial substances of sponges. II. Structure and synthesis of a bromine-containing antibacterial compound from a marine sponge. *Tetrahedron Lett.* **42,** 4147–4150 CrossRef Medline
46. Burkholder, P. R., and Sharma, G. M. (1969) Antimicrobial agents from the sea. *Lloydia* **32,** 466–483 Medline
47. Sharma, G. M., Vig, B., and Burkholder, P. R. (1970) Studies on the antimicrobial substances of sponges. IV. Structure of a bromine-containing compound from a marine sponge. *J. Org. Chem.* **35,** 2823–2826 CrossRef Medline
48. Unson, M. D., Holland, N. D., and Faulkner, D. J. (1994) A brominated secondary metabolite synthesized by the cyanobacterial symbiont of a marine sponge and accumulation of the crystalline metabolite in the sponge tissue. *Mar. Biol.* **119,** 1–11 CrossRef
49. Zhang, W., and Liu, H. T. (2002) MAPK signal pathways in the regulation of cell proliferation in mammalian cells. *Cell Res.* **12,** 9–18 CrossRef Medline
50. Li, Z., Theus, M. H., and Wei, L. (2006) Role of ERK 1/2 signaling in neuronal differentiation of cultured embryonic stem cells. *Dev. Growth Differ.* **48,** 513–523 CrossRef Medline
51. Rhim, J. H., Luo, X., Gao, D., Xu, X., Zhou, T., Li, F., Wang, P., Wong, S. T., and Xia, X. (2016) Cell type-dependent Erk–Akt pathway crosstalk regulates the proliferation of fetal neural progenitor cells. *Sci. Rep.* **6,** 26547 CrossRef Medline
52. Bülow, H. E., Boulin, T., and Hobert, O. (2004) Differential functions of the report *C. elegans* FGF receptor in axon outgrowth and maintenance of axon position. *Neuron* **42,** 367–374 CrossRef Medline
53. Tang, F., and Kalil, K. (2005) Netrin-1 induces axon branching in developing cortical neurons by frequency-dependent calcium signaling pathways. *J. Neurosci.* **25,** 6702–6715 CrossRef Medline
54. Xing, L., Larsen, R. S., Bjorklund, G. R., Li, X., Wu, Y., Philpot, B. D., Snider, W. D., and Newbern, J. M. (2016) Layer specific and general requirements for ERK/MAPK signaling in the developing neocortex. *Elife.* **5,** e11123 Medline
55. Igarashi, M., and Okuda, S. (2019) Evolutionary analysis of proline-directed phosphorylation sites in the mammalian growth cone identified using phosphoproteomics. *Mol. Brain* **12,** 53 CrossRef Medline

56. Rauen, K. A. (2013) The RASopathies. *Annu. Rev. Genomics Hum. Genet.* **14,** 355–369 CrossRef Medline
57. Millan, M. J. (2013) An epigenetic framework for neurodevelopmental disorders: from pathogenesis to potential therapy. *Neuropharmacology* **68,** 2–82 CrossRef Medline
58. Huang, E. J., and Reichardt, L. F. (2001) Neurotrophins: roles in neuronal development and function. *Annu. Rev. Neurosci.* **24,** 677–736 CrossRef Medline
59. Giachello, C. N., Fiumara, F., Giacomini, C., Corradi, A., Milanese, C., Ghirardi, M., Benfenati, F., and Montarolo, P. G. (2010) MAPK/Erk-dependent phosphorylation of synapsin mediates formation of functional synapses and short-term homosynaptic plasticity. *J. Cell Sci.* **123,** 881–893 CrossRef Medline
60. Martin, K. C., Michael, D., Rose, J. C., Barad, M., Casadio, A., Zhu, H., and Kandel, E. R. (1997) MAP kinase translocates into the nucleus of the presynaptic cell and is required for long-term facilitation in Aplysia. *Neuron* **18,** 899–912 CrossRef Medline
61. Lyons, M. R., and West, A. E. (2011) Mechanisms of specificity in neuronal activity-regulated gene transcription. *Prog. Neurobiol.* **94,** 259–295 CrossRef Medline
62. Charlesworth, P., Cotterill, E., Morton, A., Grant, S. G., and Eglen, S. J. (2015) Quantitative differences in developmental profiles of spontaneous activity in cortical and hippocampal cultures. *Neural Dev.* **10,** 1 CrossRef Medline
63. Arnold, F. J., Hofmann, F., Bengtson, C. P., Wittmann, M., Vanhoutte, P., and Bading, H. (2005) Microelectrode array recordings of cultured hippocampal networks reveal a simple model for transcription and protein synthesis-dependent plasticity. *J. Physiol.* **564,** 3–19 CrossRef Medline
64. Heald, R. A., Jackson, P., Savy, P., Jones, M., Gancia, E., Burton, B., Newman, R., Boggs, J., Chan, E., Chan, J., Choo, E., Merchant, M., Rudewicz, P., Ultsch, M., Wiesmann, C., *et al.* (2012) Discovery of novel allosteric mitogen-activated protein kinase kinase (MEK) 1,2 inhibitors possessing bidentate Ser212 interactions. *J. Med. Chem.* **55,** 4594–4604 CrossRef Medline
65. Zhao, Z., Xie, L., and Bourne, P. E. (2017) Insights into the binding mode of MEK type-III inhibitors. A step toward discovering and designing allosteric kinase inhibitors across the human kinome. *PLoS ONE* **12,** e0179936 CrossRef Medline
66. Trott, O., and Olson, A. J. (2010) AutoDock Vina: improving the speed and accuracy of docking with a new scoring function, efficient optimization, and multithreading. *J. Comput. Chem.* **31,** 455–461 CrossRef Medline
67. Guo, X., Williams, J. G., Schug, T. T., and Li, X. (2010) DYRK1A and DYRK3 promote cell survival through phosphorylation and activation of SIRT1. *J. Biol. Chem.* **285,** 13223–13232 CrossRef Medline
68. Li, Y., Xu, W., McBurney, M. W., and Longo, V. D. (2008) SirT1 inhibition reduces IGF-I/IRS-2/Ras/ERK1/2 signaling and protects neurons. *Cell Metab.* **8,** 38–48 CrossRef Medline
69. Zhao, Y., Luo, P., Guo, Q., Li, S., Zhang, L., Zhao, M., Xu, H., Yang, Y., Poon, W., and Fei, Z. (2012) Interactions between SIRT1 and MAPK/ERK regulate neuronal apoptosis induced by traumatic brain injury *in vitro* and *in vivo*. *Exp. Neurol.* **237,** 489–498 CrossRef Medline
70. Schmitt, J. M., Wayman, G. A., Nozaki, N., and Soderling, T. R. (2004) Calcium activation of ERK mediated by calmodulin kinase I. *J. Biol. Chem.* **279,** 24064–24072 CrossRef Medline
71. Schmitt, J. M., Guire, E. S., Saneyoshi, T., and Soderling, T. R. (2005) Calmodulin-dependent kinase kinase/calmodulin kinase I activity gates extracellular-regulated kinase-dependent long-term potentiation. *J. Neurosci.* **25,** 1281–1290 CrossRef Medline
72. Wayman, G. A., Impey, S., Marks, D., Saneyoshi, T., Grant, W. F., Derkach, V., and Soderling, T. R. (2006) Activity-dependent dendritic arborization mediated by CaM-kinase I activation and enhanced CREB-dependent transcription of Wnt-2. *Neuron* **50,** 897–909 CrossRef Medline
73. Ageta-Ishihara, N., Takemoto-Kimura, S., Nonaka, M., Adachi-Morishima, A., Suzuki, K., Kamijo, S., Fujii, H., Mano, T., Blaeser, F., Chatila, T. A., Mizuno, H., Hirano, T., Tagawa, Y., Okuno, H., and Bito, H. (2009) Control of cortical axon elongation by a GABA-driven Ca^{2+}/calmodulin-dependent protein kinase cascade. *J. Neurosci.* **29,** 13720–13729 CrossRef Medline
74. Cesca, F., Baldelli, P., Valtorta, F., and Benfenati, F. (2010) The synapsins: key actors of synapse function and plasticity. *Prog. Neurobiol.* **91,** 313–348 CrossRef Medline
75. Samuels, I. S., Saitta, S. C., and Landreth, G. E. (2009) MAP'ing CNS development and cognition: an ERKsome process. *Neuron* **61,** 160–167 CrossRef Medline
76. Wayman, G. A., Kaech, S., Grant, W. F., Davare, M., Impey, S., Tokumitsu, H., Nozaki, N., Banker, G., and Soderling, T. R. (2004) Regulation of axonal extension and growth cone motility by calmodulin-dependent protein kinase I. *J. Neurosci.* **24,** 3786–3794 CrossRef Medline
77. Takemoto-Kimura, S., Ageta-Ishihara, N., Nonaka, M., Adachi-Morishima, A., Mano, T., Okamura, M., Fujii, H., Fuse, T., Hoshino, M., Suzuki, S., Kojima, M., Mishina, M., Okuno, H., and Bito, H. (2007) Regulation of dendritogenesis via a lipid-raft-associated Ca^{2+}/calmodulin-dependent protein kinase CLICK-III/CaMKIγ. *Neuron* **54,** 755–770 CrossRef Medline
78. Kim, K., Cha, J. S., Cho, Y.-S., Kim, H., Chang, N., Kim, H.-J., and Cho, H.-S. (2018) Crystal structure of human dual-specificity tyrosine-regulated kinase 3 reveals new structural features and insights into its autophosphorylation. *J. Mol. Biol.* **430,** 1521–1530 CrossRef Medline
79. Michel, C. I., Kraft, R., and Restifo, L. L. (2004) Defective neuronal development in the mushroom bodies of drosophila fragile X mental retardation 1 mutants. *J. Neurosci.* **24,** 5798–5809 CrossRef Medline
80. Brown, J. P., Hall, D., Frank, C. L., Wallace, K., Mundy, W. R., and Shafer, T. J. (2016) Evaluation of a microelectrode array-based assay for neural network ontogeny using training set chemicals. *Toxicol. Sci.* **154,** 126–139 CrossRef Medline
81. Frank, C. L., Brown, J. P., Wallace, K., Mundy, W. R., and Shafer, T. J. (2017) Developmental neurotoxicants disrupt activity in cortical networks on microelectrode arrays: results of screening 86 compounds during neural network formation. *Toxicol. Sci.* **160,** 121–135 CrossRef Medline
82. Shafer, T. J., Brown, J. P., Lynch, B., Davila-Montero, S., Wallace, K., and Friedman, K. P. (2019) Evaluation of chemical effects on network formation in cortical neurons grown on microelectrode arrays. *Toxicol. Sci.* **169,** 436–455 CrossRef Medline
83. Schenk, U., Menna, E., Kim, T., Passafaro, M., Chang, S., De Camilli, P., and Matteoli, M. (2005) A novel pathway for presynaptic mitogen-activated kinase activation via AMPA receptors. *J. Neurosci.* **25,** 1654–1663 CrossRef Medline
84. Vara, H., Onofri, F., Benfenati, F., Sassoè-Pognetto, M., and Giustetto, M. (2009) ERK activation in axonal varicosities modulates presynaptic plasticity in the CA3 region of the hippocampus through synapsin I. *Proc. Natl. Acad. Sci. U.S.A.* **106,** 9872–9877 CrossRef Medline
85. Malmberg, T., Athanasiadou, M., Marsh, G., Brandt, I., and Bergman, A. (2005) Identification of hydroxylated polybrominated diphenyl ether metabolites in blood plasma from polybrominated diphenyl ether exposed rats. *Environ. Sci. Technol.* **39,** 5342–5348 CrossRef Medline
86. Lupton, S. J., McGarrigle, B. P., Olson, J. R., Wood, T. D., and Aga, D. S. (2009) Human liver microsome-mediated metabolism of brominated diphenyl ethers 47, 99, and 153 and identification of their major metabolites. *Chem. Res. Toxicol.* **22,** 1802–1809 CrossRef Medline
87. Miksys, S., and Tyndale, R. F. (2004) The unique regulation of brain cytochrome P450 2 (CYP2) family enzymes by drugs and genetics. *Drug Metab. Rev.* **36,** 313–333 CrossRef Medline
88. Plotnikov, A., Zehorai, E., Procaccia, S., and Seger, R. (2011) The MAPK cascades: signaling components, nuclear roles and mechanisms of nuclear translocation. *Biochim. Biophys. Acta* **1813,** 1619–1633 CrossRef Medline
89. Zhou, F.-Q., and Snider, W. D. (2006) Intracellular control of developmental and regenerative axon growth. *Philos. Trans. R. Soc. Lond. B Biol. Sci.* **361,** 1575–1592 CrossRef Medline
90. Chen, H., Streifel, K. M., Singh, V., Yang, D., Mangini, L., Wulff, H., and Lein, P. J. (2017) BDE-47 and BDE-49 inhibit axonal growth in primary rat hippocampal neuron–glia co-cultures via ryanodine receptor-dependent mechanisms. *Toxicol. Sci.* **156,** 375–386 CrossRef Medline

91. Lake, D., Corrêa, S. A., and Müller, J. (2016) Negative feedback regulation of the ERK1/2 MAPK pathway. *Cell. Mol. Life Sci.* **73,** 4397–4413 CrossRef Medline
92. Li, T., Wang, W., Pan, Y. W., Xu, L., and Xia, Z. (2013) A hydroxylated metabolite of flame-retardant PBDE-47 decreases the survival, proliferation, and neuronal differentiation of primary cultured adult neural stem cells and interferes with signaling of ERK5 MAP kinase and neurotrophin 3. *Toxicol. Sci.* **134,** 111–124 CrossRef Medline
93. Chen, H., Guo, R., Zhang, Q., Guo, H., Yang, M., Wu, Z., Gao, S., Liu, L., and Chen, L. (2015) Erk signaling is indispensable for genomic stability and self-renewal of mouse embryonic stem cells. *Proc. Natl. Acad. Sci. U.S.A.* **112,** E5936–E5943 CrossRef Medline
94. Huang, S. C., Giordano, G., and Costa, L. G. (2010) Comparative cytotoxicity and intracellular accumulation of five polybrominated diphenyl ether congeners in mouse cerebellar granule neurons. *Toxicol. Sci.* **114,** 124–132 CrossRef Medline
95. Wortzel, I., and Seger, R. (2011) The ERK cascade: distinct functions within various subcellular organelles. *Genes Cancer* **2,** 195–209 CrossRef Medline
96. Mao, L.-M., and Wang, J. Q. (2016) Synaptically localized mitogen-activated protein kinases: local substrates and regulation. *Mol. Neurobiol.* **53,** 6309–6315 CrossRef Medline
97. Yang, J. H., Mao, L.-M., Choe, E. S., and Wang, J. Q. (2017) Synaptic ERK2 phosphorylates and regulates metabotropic glutamate receptor 1 *in vitro* and in neurons. *Mol. Neurobiol.* **54,** 7156–7170 CrossRef Medline
98. Jovanovic, J. N., Benfenati, F., Siow, Y. L., Sihra, T. S., Sanghera, J. S., Pelech, S. L., Greengard, P., and Czernik, A. J. (1996) Neurotrophins stimulate phosphorylation of synapsin I by MAP kinase and regulate synapsin I-actin interactions. *Proc. Natl. Acad. Sci.* **93,** 3679–3683 CrossRef Medline
99. Kushner, S. A., Elgersma, Y., Murphy, G. G., Jaarsma, D., van Woerden, G. M., Hojjati, M. R., Cui, Y., LeBoutillier, J. C., Marrone, D. F., Choi, E. S., De Zeeuw, C. I., Petit, T. L., Pozzo-Miller, L., and Silva, A. J. (2005) Modulation of presynaptic plasticity and learning by the H-ras/extracellular signal-regulated kinase/synapsin I signaling pathway. *J. Neurosci.* **25,** 9721–9734 CrossRef Medline
100. Semprich, C. I., Metzis, V., Patel, H., Briscoe, J., and Storey, K. G. (2019) ERK1/2 signalling dynamics promote neural differentiation by regulating the polycomb repressive complex. *bioRxiv* CrossRef
101. Chen, Y., Stevens, B., Chang, J., Milbrandt, J., Barres, B. A., and Hell, J. W. (2008) NS21: re-defined and modified supplement B27 for neuronal cultures. *J. Neurosci. Methods* **171,** 239–247 CrossRef Medline
102. Bardy, C., van den Hurk, M., Eames, T., Marchand, C., Hernandez, R. V., Kellogg, M., Gorris, M., Galet, B., Palomares, V., Brown, J., Bang, A. G., Mertens, J., Böhnke, L., Boyer, L., Simon, S., and Gage, F. H. (2015) Neuronal medium that supports basic synaptic functions and activity of human neurons *in vitro*. *Proc. Natl. Acad. Sci. U.S.A.* **112,** E2725–E2734 CrossRef Medline
103. Fischmann, T. O., Smith, C. K., Mayhood, T. W., Myers, J. E., Reichert, P., Mannarino, A., Carr, D., Zhu, H., Wong, J., Yang, R.-S., Le, H. V., and Madison, V. S. (2009) Crystal structures of MEK1 binary and ternary complexes with nucleotides and inhibitors. *Biochemistry* **48,** 2661–2674 CrossRef Medline
104. Zha, M., Zhong, C., Ou, Y., Han, L., Wang, J., and Ding, J. (2012) Crystal structures of human CaMKIα reveal insights into the regulation mechanism of CaMKI. *PLoS ONE* **7,** e44828 CrossRef Medline
105. Agnew, C., Liu, L., Liu, S., Xu, W., You, L., Yeung, W., Kannan, N., Jablons, D., and Jura, N. (2019) The crystal structure of the protein kinase HIPK2 reveals a unique architecture of its CMGC-insert region. *J. Biol. Chem.* **294,** 13545–13559 CrossRef Medline
106. Barf, T., Kaptein, A., de Wilde, S., van der Heijden, R., van Someren, R., Demont, D., Schultz-Fademrecht, C., Versteegh, J., van Zeeland, M., Seegers, N., Kazemier, B., van de Kar, B., van Hoek, M., de Roos, J., Klop, H., *et al.* (2011) Structure-based lead identification of ATP-competitive MK2 inhibitors. *Bioorg. Med. Chem. Lett.* **21,** 3818–3822 CrossRef Medline
107. Kumar, A., Mandiyan, V., Suzuki, Y., Zhang, C., Rice, J., Tsai, J., Artis, D. R., Ibrahim, P., and Bremer, R. (2005) Crystal structures of proto-oncogene kinase Pim1: a target of aberrant somatic hypermutations in diffuse large cell lymphoma. *J. Mol. Biol.* **348,** 183–193 CrossRef Medline
108. Forli, S., Huey, R., Pique, M. E., Sanner, M. F., Goodsell, D. S., and Olson, A. J. (2016) Computational protein–ligand docking and virtual drug screening with the AutoDock suite. *Nat. Protoc.* **11,** 905–919 CrossRef Medline
109. Ohren, J. F., Chen, H., Pavlovsky, A., Whitehead, C., Zhang, E., Kuffa, P., Yan, C., McConnell, P., Spessard, C., Banotai, C., Mueller, W. T., Delaney, A., Omer, C., Sebolt-Leopold, J., Dudley, D. T., *et al.* (2004) Structures of human MAP kinase kinase 1 (MEK1) and MEK2 describe novel noncompetitive kinase inhibition. *Nat. Struct. Mol. Biol.* **11,** 1192–1197 CrossRef Medline
110. Hastie, C. J., McLauchlan, H. J., and Cohen, P. (2006) Assay of protein kinases using radiolabeled ATP: a protocol. *Nat. Protoc.* **1,** 968–971 CrossRef Medline
111. Bain, J., Plater, L., Elliott, M., Shpiro, N., Hastie, C. J., McLauchlan, H., Klevernic, I., Arthur, J. S., Alessi, D. R., and Cohen, P. (2007) The selectivity of protein kinase inhibitors: a further update. *Biochem. J.* **408,** 297–315 CrossRef Medline